

Weakly subcritical stationary patterns: Eckhaus instability and homoclinic snaking

Hsien-Ching Kao* and Edgar Knobloch†

Department of Physics, University of California, Berkeley, California 94720, USA

(Received 23 September 2011; published 21 February 2012)

The transition from subcritical to supercritical stationary periodic patterns is described by the one-dimensional cubic-quintic Ginzburg-Landau equation $A_t = \mu A + A_{xx} + i(a_1|A|^2 A_x + a_2 A^2 A_x^*) + b|A|^2 A - |A|^4 A$, where $A(x, t)$ represents the pattern amplitude and the coefficients μ , a_1 , a_2 , and b are real. The conditions for Eckhaus instability of periodic solutions are determined, and the resulting spatially modulated states are computed. Some of these evolve into spatially localized structures in the vicinity of a Maxwell point, while others resemble defect states. The results are used to shed light on the behavior of localized structures in systems exhibiting homoclinic snaking during the transition from subcriticality to supercriticality.

DOI: [10.1103/PhysRevE.85.026211](https://doi.org/10.1103/PhysRevE.85.026211)

PACS number(s): 47.54.-r, 47.20.Ky, 47.55.P-, 82.40.Ck

I. INTRODUCTION

Recent interest in spatially localized structures and their organization in bifurcation diagrams exhibiting homoclinic snaking [1,2] has motivated the study of a number of different model systems. Such model systems have proved to be of great value in interpreting the results obtained either by direct numerical simulation or numerical continuation methods on much more complex equations such as those arising in fluid dynamics [3], nonlinear optics [4], and chemical reaction kinetics [5]. Of these, the Swift-Hohenberg equation in its various versions has proved to be the most useful [6]. This equation is a fourth-order partial differential equation (PDE) for a real order parameter $u(x, t)$ on the real line. Spatially localized solutions are located in the subcritical regime that forms in the presence of competing nonlinearities and lie on two or four solution branches that bifurcate from the homogeneous solution $u = 0$ simultaneously with a (subcritical) branch of spatially periodic states [6]. In domains of large but finite period the localized states no longer bifurcate from $u = 0$ but bifurcate instead from the subcritical periodic solutions in a secondary bifurcation [7]. In large domains this bifurcation occurs at small but finite amplitude and is the result of a modulational instability called the Eckhaus instability. As one follows the resulting branches of localized states into the pinning or snaking region, the states first become strongly localized and thereafter grow in length by repeatedly nucleating new cells at either end as the solution branches begin to oscillate back and forth across the snaking region. In a finite domain this process cannot go on forever, and when the domain is almost full the branches exit the snaking region and terminate either on the branch of periodic states from which they initially bifurcated or on a different one. In each case the branches terminate in another Eckhaus bifurcation, and theory shows that the Eckhaus bifurcation of interest is always the one closest to the fold (saddle node) on the periodic state [8]. The details of this process are complex and depend on the period Γ of the domain and, more specifically, on $\Gamma \bmod \lambda_c$, where λ_c is the wavelength of the periodic states at onset [7].

The above issues become simpler within the cubic-quintic Ginzburg-Landau equation for stationary wave trains. This equation describes the evolution of the *amplitude* A of a spatially periodic state with critical wave number k_c : $u(x, t) = \epsilon A(X, T) \exp i k_c x + \text{c.c.} + \text{h.o.t.}$ Here $X = \epsilon^2 x$ and $T = \epsilon^4 t$ are slow spatial and temporal scales, and $\epsilon \ll 1$ measures the distance from threshold, taken to be of order ϵ^4 . Thus, the branch of periodic states is now identified with the *homogeneous* state $|A| \neq 0$. Within this equation nonadiabatic effects are absent and the snaking region collapses into a point identified in gradient systems with the Maxwell point, defined as the point at which the free energy associated with the state $|A| \neq 0$ vanishes. The nonadiabatic terms describe the pinning between the fronts bounding the structure on either side and the pattern within and thereby generate homoclinic snaking centered on the Maxwell point [9,10]. However, despite their absence, the cubic-quintic Ginzburg-Landau equation retains the essential properties of spatially localized states, including their origin and termination. In addition, it applies to systems that are not of gradient type. Thus, the cubic-quintic Ginzburg-Landau equation provides much useful information about the location of the pinning or snaking region in both gradient and nongradient systems, and their behavior outside of this region, as described further below.

Within the supercritical cubic Ginzburg-Landau equation, localized structures are absent but Eckhaus instabilities remain of fundamental importance since they define the wave-number interval around the band center k_c within which spatially periodic solutions with wave number k are stable. On the real line, this wave-number interval shrinks to zero the closer one approaches the primary bifurcation [11], i.e., the threshold for instability of the trivial state $|A| = 0$. The theory has been extended to periodic domains with a finite period [12,13]. In this case the allowed wave numbers are discrete and the wave number closest to the band center is stable, with the wave numbers on either side Eckhaus unstable.

In the present paper, we are interested in Eckhaus instabilities in the subcritical case. In this case, one expects on physical grounds the presence of fifth-order terms in the Ginzburg-Landau equation. Such terms prevent possible runaway of spatially homogeneous states and may be brought into the theory via a systematic expansion that treats the coefficient of the cubic term as a small quantity whose magnitude is linked

*hckao@berkeley.edu

†knobloch@berkeley.edu

to the modulation length scale of the pattern. A systematic study of this problem reveals the presence, in general, of two additional terms that come in at the same order in perturbation theory as the quintic term [14,15]. These terms have been computed explicitly from the quadratic-cubic Swift-Hohenberg equation [6,16] but are present in related computations going back a number of years [17–20]. These additional terms take the form $i|A|^2A_x$ and $iA^2A_x^*$ and substantially affect the properties of the resulting amplitude equation. In particular, the latter term renders the dynamics nonvariational, in contrast to the variational evolution familiar from the supercritical cubic Ginzburg-Landau equation. Although the resulting equation has been studied from a geometric point of view [14,18], in the present paper we seek explicit predictions in the form of bifurcation diagrams that can be directly applied to systems such as magnetoconvection in which the direction of branching changes from subcritical to supercritical as the magnetic Prandtl number increases [21].

The paper is organized as follows. In Sec. II we introduce the cubic-quintic Ginzburg-Landau equation for stationary wave trains in its general form. In Sec. III we employ spatial dynamics to show that steady solutions are completely determined by two conserved quantities. We use these quantities to gain insight into the solution structure and to identify a large variety of homoclinic and heteroclinic orbits described by this equation. In Sec. IV we study the stationary solutions of this equation that bifurcate from the primary branches of spatially periodic states, and in Sec. V we relate these results to those from conventional Eckhaus instability analysis and determine the stability properties of the solutions found in Sec. III and Sec. IV. The paper concludes with brief remarks in Sec. VI. Certain details of the analysis are relegated to three appendices.

II. THE CUBIC-QUINTIC GINZBURG-LANDAU EQUATION

We consider the evolution of the complex amplitude A of a wave train with wave number k_c near a steady-state pattern-forming instability of a homogeneous state, i.e., we write a real field variable in the form,

$$u(x,t) = \epsilon A(\epsilon^2 x, \epsilon^4 t) e^{ik_c x} + \text{c.c.} + \text{h.o.t.} \quad (1)$$

The scaling of the amplitude A is a consequence of choosing the coefficient of the term $|A|^2 A$ to be $O(\epsilon^2)$, a condition that permits us to bring fifth-order terms self-consistently into the theory. These terms are in turn required to stabilize solutions when the primary bifurcation is subcritical. The resulting theory is thus a codimension-two description of the bifurcation of steady wave trains. Multiple-scale analysis now leads to an amplitude equation of the form [15,17]

$$A_t = \mu A + A_{xx} + i(a_1 |A|^2 A_x + a_2 A^2 A_x^*) + b |A|^2 A - |A|^4 A, \quad (2)$$

where μ and b are real $O(1)$ unfolding parameters, a_1 and a_2 are two real $O(1)$ coefficients that can be positive or negative, and the variables x and t now refer to $\epsilon^2 x$ and $\epsilon^4 t$, respectively. The coefficients of A , A_{xx} and of the quintic term can always be set equal to 1 by a suitable rescaling of t , x , and A . However, μ represents the bifurcation

parameter and hence is retained in what follows. In unscaled variables all terms in this equation are of fifth order, with $\epsilon^4 \mu$ denoting the distance from the bifurcation point. An equation of this type can be derived from the quadratic-cubic Swift-Hohenberg equation near the primary pattern-forming instability [6,16]. The derivation provides explicit expressions for the coefficients and, moreover, shows that a term of the form iA_x may also be present on the right side of Eq. (2). See also Ref. [19]. We mention that the envelope description is valid, provided $|A| > 0$ throughout the domain. The spatial phase of the wave train (1) becomes undefined at zeros of $|A|$; thus, zeros of $|A|$ are generally associated with the presence of phase jumps.

Equation (2) has been studied before. For example, its primary steady states and their properties were studied by Doelman and Eckhaus [14] in the special case $b = 0$ and by Shepeleva [22] when $b \neq 0$. See also Refs. [18,23,24]. However, despite these papers, our understanding of secondary solution branches and their stability properties remains incomplete. In particular, we focus in the following on the properties of fully nonlinear spatially modulated states in finite domains and on the role played by the Maxwell point in the process of wave-number selection. Our results, including stability properties, are presented in the form of bifurcation diagrams describing the transitions among the different states as the bifurcation parameter μ varies. Our results can be used to make predictions about the fate of spatially localized structures during the transition from subcriticality to supercriticality, i.e., as b passes through zero.

We begin by noting that Eq. (2) is equivariant under the three operations:

- (i) $x \rightarrow x, \quad A \rightarrow A e^{i\phi_0}$,
- (ii) $x \rightarrow x + x_0, \quad A \rightarrow A$,
- (iii) $x \rightarrow x_1 - x, \quad A \rightarrow A^*$,

where ϕ_0 , x_0 , and x_1 are arbitrary constants. The first two operations are a consequence of translation invariance of the underlying problem, while the third arises when the underlying system is invariant under reflections. In this case the coefficients μ , a_1 , a_2 , and b in Eq. (2) must all be real. The symmetry (iii) renders Eq. (2) *spatially reversible*.

When $a_2 = 0$, Eq. (2) has gradient structure,

$$A_t = - \frac{\delta F(A, A^*)}{\delta A^*}, \quad (3)$$

where

$$F(A, A^*) = \int_{\Gamma} \left\{ |A_x|^2 - \mu |A|^2 - \frac{b|A|^4}{2} + \frac{|A|^6}{3} + \frac{ia_1}{4} |A|^2 (A A_x^* - A^* A_x) \right\} dx \quad (4)$$

and Γ is either the whole real line or a finite closed interval. In particular, in the latter case, all solutions approach a time-independent state corresponding to a local minimum of the free energy $F(A, A^*)$ provided F is bounded from below. However, this is not necessarily the case. In fact, the lower bound on F

is finite only when $|a_1| < \frac{4}{\sqrt{3}}$. This result follows from the estimate

$$F \geq \int_{\Gamma} \left\{ |A_x|^2 - \mu |A|^2 - \frac{b|A|^4}{2} + \frac{|A|^6}{3} - \frac{|a_1|}{2} |A|^3 |A_x| \right\} dx, \quad (5)$$

which in turn implies, using Young's inequality, that

$$F \geq \int_{\Gamma} \left\{ \left(1 - \frac{|a_1|}{4\delta}\right) |A_x|^2 + \left(\frac{1}{3} - \frac{|a_1|\delta}{4}\right) |A|^6 - \mu |A|^2 - \frac{b|A|^4}{2} \right\} dx \quad (6)$$

for all $\delta > 0$. It follows that if the domain size is finite and $1 - \frac{|a_1|}{4\delta}$ and $\frac{1}{3} - \frac{|a_1|\delta}{4}$ are both positive, i.e., $|a_1| < \frac{4}{\sqrt{3}}$, then F is bounded from below. However, when $|a_1| > \frac{4}{\sqrt{3}}$, this is no longer so. To see this we note that the integrand for periodic wave trains of the form $A = R_0 \exp ikx$, where R_0 is a constant, reduces to

$$R_0^2 k^2 - \mu R_0^2 - \frac{b}{2} R_0^4 + \frac{R_0^6}{3} + \frac{a_1 k R_0^4}{2} \approx R_0^2 \left(k + \frac{a_1 R_0^2}{4} \right)^2 + \left(\frac{1}{3} - \frac{a_1^2}{16} \right) R_0^6$$

for large R_0 . Thus, for $|a_1| > \frac{4}{\sqrt{3}}$ the free energy F of wave trains with $k = -\frac{1}{4} a_1 R_0^2$ diverges to negative infinity as $R_0 \rightarrow \infty$, thereby permitting the existence of runaway solutions.

The situation is yet more interesting when a_2 is nonzero since no free energy then exists and the time evolution of the system need not be monotonic. Thus, the presence of the terms $ia_1 |A|^2 A_x$ and $ia_2 A^2 A_x^*$ in the amplitude equation changes qualitatively the evolution of the system near the pattern-forming bifurcation. In particular, oscillations may now be present [22], and these may be expected near the saddle node on the primary solution branch, where the growth rates of the amplitude and phase modes are both small and, hence, comparable.

We remark that for the quadratic-cubic Swift-Hohenberg equation $(a_1, a_2) = (\frac{4}{21\sqrt{3}}, 0)$ [16]. Thus, F is bounded from below and oscillations are absent. The latter is, of course, a consequence of the gradient structure of the equation.

III. STATIONARY SOLUTIONS

Stationary solutions of Eq. (2) satisfy the equation

$$A_{xx} + i(a_1 |A|^2 A_x + a_2 A^2 A_x^*) + \mu A + b|A|^2 A - |A|^4 A = 0. \quad (7)$$

In the following, we view this equation as a fourth-order (real) dynamical system in space. In view of the two continuous symmetries associated with translations and phase shifts the equation has two conserved quantities [14]

$$E \equiv (\mu + 2a_2 L) |A|^2 + |A_x|^2 + \frac{b}{2} |A|^4 - \left[\frac{1}{3} + \frac{a_2(a_1 + a_2)}{6} \right] |A|^6, \quad (8)$$

$$L \equiv \frac{i}{2} (AA_x^* - A^* A_x) + \frac{a_1 + a_2}{4} |A|^4. \quad (9)$$

In terms of $A(x) = R(x)e^{i\phi(x)}$, where $R(x)$ and $\phi(x)$ are real-valued functions, these take the form

$$E = (\mu + 2a_2 L) R^2 + (R_x^2 + R^2 \phi_x^2) + \frac{b}{2} R^4 - \left[\frac{1}{3} + \frac{a_2(a_1 + a_2)}{6} \right] R^6, \quad (10)$$

$$L = R^2 \phi_x + \frac{a_1 + a_2}{4} R^4. \quad (11)$$

Thus,

$$R_x^2 + U = E, \quad (12)$$

where

$$U(R; \mu, L) \equiv \frac{L^2}{R^2} + \left(\mu + \frac{3a_2 - a_1}{2} L \right) R^2 + \frac{b}{2} R^4 + \beta R^6 \quad (13)$$

and $\beta \equiv \frac{(a_1 + a_2)^2}{16} - \frac{a_2(a_1 + a_2)}{6} - \frac{1}{3}$ [14]. The problem (7) has thus been reduced to that of a particle of energy E in a potential U . The form of the potential depends on the integral L as well as on the bifurcation parameter μ . Thus solutions of Eq. (12) come in two-parameter families, specified by the values of E and L . In general, the solution of Eq. (12) will be a periodic function of x . In view of the fact that $\phi_x = (L/R^2) - \frac{1}{4}(a_1 + a_2)R^2$, this solution corresponds to a complex amplitude $A(x)$ with two frequencies, one associated with oscillations in the amplitude $R(x)$ and the other with oscillations in the spatial phase $\phi(x)$. In the following we refer to such solutions as *two frequency* states, while noting that in periodic domains with finite spatial period the two frequencies must be rationally related. In the following, we write $\phi_x \equiv k$ and refer to k as the wave number. Of particular interest are equilibria of Eq. (12) with $R = R_0$, where R_0 is a constant. If the associated $\phi_x \equiv k \neq 0$, such a solution corresponds to a wave of constant amplitude R_0 . We call such solutions rotating waves (RW) by analogy with the corresponding solution in the time domain, cf. Refs. [25,26]. Likewise, periodic solutions of Eq. (12) with $k = 0$ will be called standing waves (SW). Both solution types are single-frequency states. We mention that equilibria with $k = 0$ correspond in the original problem [Eq. (1)] to periodic wave trains with wave number k_c , while equilibria with $k \neq 0$ (i.e., RW) correspond to periodic wave trains with wave number $k_c + k$. In contrast, SW correspond to spatially modulated wave trains. Finally, homoclinic and heteroclinic orbits correspond to spatially localized states and fronts, respectively.

The notion of stability within Eq. (7) refers to *spatial* stability. In particular, the loss of stability of an equilibrium corresponds to the appearance of new steady states with an x -dependent amplitude R and phase ϕ . Such bifurcations occur at amplitudes R_0 defined by $U_R = 0$ and satisfying $U_{RR} > 0$, where

$$U_{RR} = 8k^2 + 4[b + (a_1 + a_2)k]R_0^2 + 2(a_1^2 - a_2^2 - 4)R_0^4. \quad (14)$$

To demonstrate this result, we write $A = (R_0 + r) \exp i(kx + \phi_0 + \psi)$ and take $|r| \ll 1$, $|\psi| \ll 1$. The linearized system of

equations governing the evolution of the perturbations r and ψ is then given by

$$\frac{d}{dx} \begin{pmatrix} r \\ s \\ \psi \\ q \end{pmatrix} = \begin{pmatrix} 0 & 1 & 0 & 0 \\ -\frac{1}{2}(U_{RR} + U_{RL} \frac{\partial L}{\partial R}) & 0 & -\frac{U_{RL}}{2} \frac{\partial L}{\partial k} & 0 \\ 0 & 0 & 1 & 0 \\ 0 & -\frac{1}{R^2} \frac{\partial L}{\partial R} & 0 & 0 \end{pmatrix} \begin{pmatrix} r \\ s \\ \psi \\ q \end{pmatrix}, \quad (15)$$

where the coefficients are all evaluated at $R = R_0$ and $\phi_x = k$. The associated spatial eigenvalues and eigenvectors are

$$\lambda_{1,2} = 0, v_{1,2} = \begin{pmatrix} 0 \\ 0 \\ 1 \\ 0 \end{pmatrix}; \quad \lambda_{3,4} = \pm \sqrt{-\frac{U_{RR}}{2}},$$

$$v_{3,4} = \begin{pmatrix} \pm \sqrt{-U_{RR}/2} \\ -U_{RR}/2 \\ -\frac{1}{R^2} \frac{\partial L}{\partial R} \\ \mp \frac{1}{R^2} \frac{\partial L}{\partial R} \sqrt{-U_{RR}/2} \end{pmatrix}.$$

The equilibrium is elliptic when $U_{RR} > 0$ and hyperbolic when $U_{RR} < 0$. The degenerate solution with $U_R = U_{RR} = 0$ is, in general, a saddle but can be elliptic if $U_{RRR} = 0$, $U_{RRRR} > 0$. Such an equilibrium is given by $R_0^2 = -\frac{b}{8\beta}$ and occurs when $b = -8(L^2\beta^3)^{1/4}$ and $\mu + \frac{3a_2 - a_1}{2}L = 6(L^2\beta)^{1/2}$, where $\beta > 0$ and, hence, $b < 0$. When the energy E is increased above that for a local minimum, periodic solutions bifurcate from the elliptic equilibrium, and these correspond to quasiperiodic wave trains whose amplitude oscillates with spatial period close to $2\pi\sqrt{2/U_{RR}}$.

We begin with the equilibria $R = R_0(k)$. With $\phi_x \equiv k$ these satisfy the polynomial equation

$$\mu - k^2 + [b + k(a_2 - a_1)]R_0^2 - R_0^4 = 0. \quad (16)$$

Thus, homogeneous states $k = 0$ set in first as μ increases, followed by spatially inhomogeneous RW at $\mu = k^2$. The amplitude R_0 of these states is given by the roots R_0^\pm of this equation,

$$(R_0^\pm)^2 \equiv \frac{1}{2}[b' \pm \sqrt{b'^2 + 4(\mu - k^2)}], \quad (17)$$

where $b' \equiv b + k(a_2 - a_1)$. Thus, when $b' \leq 0$ (the supercritical case), only the R_0^+ solution exists and it bifurcates supercritically from the trivial state at $\mu = k^2$. This solution is stable (in time) with respect to amplitude perturbations, i.e., perturbations with the same wave number k as the solution. When $b' > 0$ (the subcritical case), a saddle-node bifurcation occurs at $\mu_{\text{sn}}(k) \equiv k^2 - \frac{b'^2}{4}$, creating both R_0^- and R_0^+ solutions, with R_0^- unstable and R_0^+ stable. The R_0^- branch connects to the trivial state at $\mu = k^2$ via a subcritical bifurcation. When $(a_2 - a_1)^2 - 4 < 0$, the curve $\mu = \mu_{\text{sn}}(k)$ has positive curvature, leading to a modest interval of bistability [Fig. 1(a)], and under this condition the global existence of solutions has been proved [27]. In contrast, when $(a_2 - a_1)^2 - 4 > 0$, the curve $\mu = \mu_{\text{sn}}(k)$ has negative curvature, leading to a subcritical region that broadens rapidly with increasing wave number k [Fig. 1(b)]. These differences are reflected in the bifurcation diagrams at fixed k shown in Fig. 2 and, more dramatically, in bifurcation diagrams constructed for fixed $\mu > 0$ [Figs. 3(a) and 3(b)] and $\mu < 0$ [Figs. 3(c) and 3(d)], cf. Ref. [14]. The lines $|a_2 - a_1| = 2$ in the (a_1, a_2) plane are shown in Fig. 4 and are tangent to the curve $\beta = 0$ at the points $(a_1, a_2) = (\pm\sqrt{3}, 1)$.

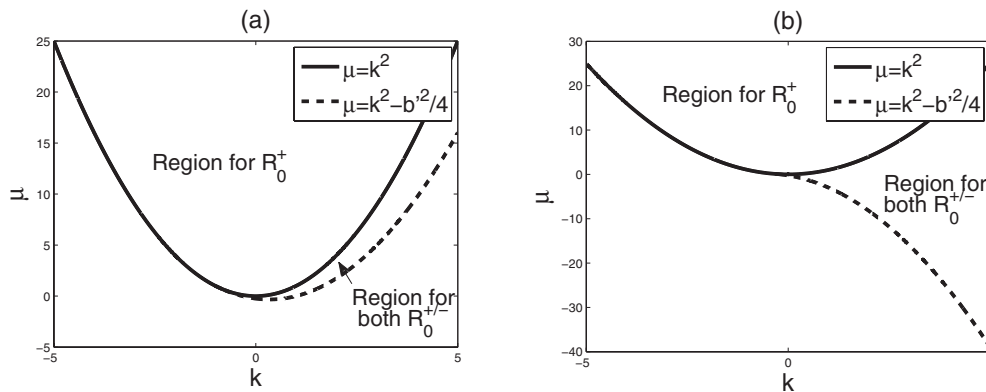


FIG. 1. The existence region in parameter space of periodic states when (a) $a_2 - a_1 = 1$, $b = 1$, and (b) $a_2 - a_1 = 3$, $b = 1$. In both cases the state R_0^+ exists for $\mu > k^2$ if $b' < 0$ and for $\mu > k^2 - \frac{b'^2}{4}$ if $b' \geq 0$; R_0^- exists in the region between $\mu = k^2$ and $\mu = k^2 - \frac{b'^2}{4}$, but the curve $\mu = k^2 - \frac{b'^2}{4}$ in (a) and (b) has positive (negative) curvature depending on the sign of $(a_2 - a_1)^2 - 4$.

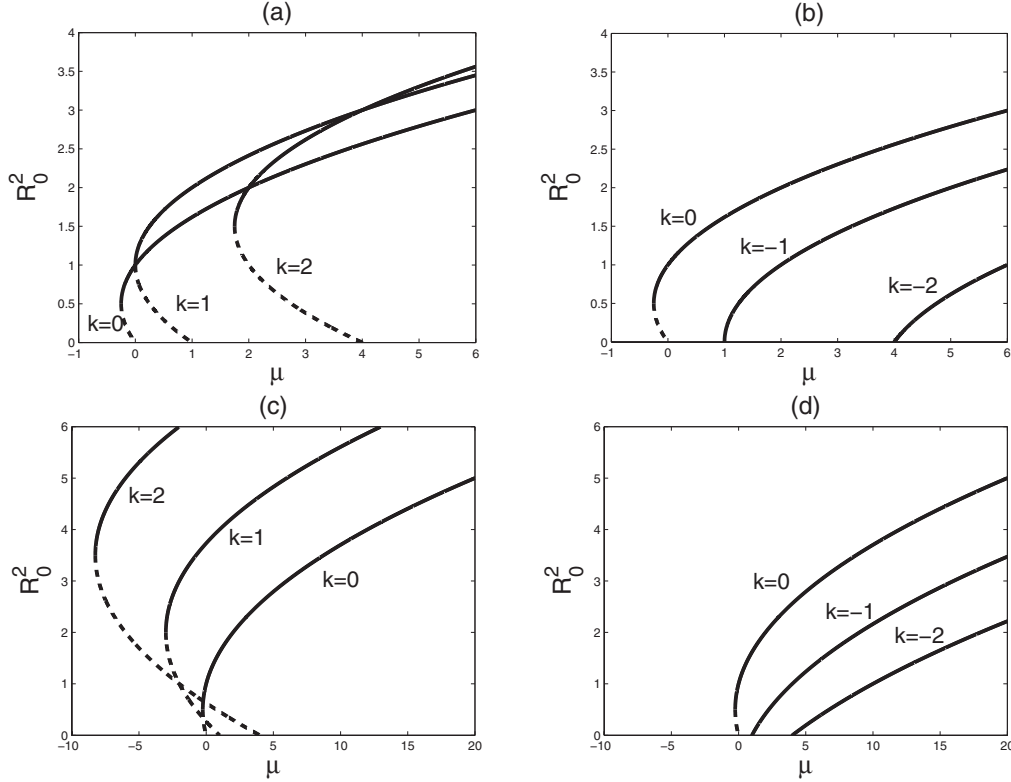


FIG. 2. Bifurcation diagrams showing R_0^2 as a function of μ for [(a) and (b)] $|a_2 - a_1| < 2$, [(c) and (d)] $|a_2 - a_1| > 2$. Panels (a) and (b) are for $a_2 - a_1 = 1$, $b = 1$ and show (a) $k \geq 0$ and (b) $k \leq 0$. Panels (c) and (d) are for $a_2 - a_1 = 3$, $b = 1$ and show (c) $k \geq 0$ and (d) $k \leq 0$. Solid (dashed) lines indicate solutions that are stable (unstable) in time with respect to amplitude perturbations. These correspond to R_0^+ and R_0^- , respectively.

Different types of spatially modulated states can be determined by examining the shape of the potential $U(R; \mu, L)$. Figures 5–6 classify the possibilities for $L = 0$ and $L > 0$, respectively. The $L < 0$ case can be obtained from $L > 0$ by changing the signs of a_1 and a_2 . These results allow us to identify different types of homoclinic and heteroclinic orbits that play an important role in what follows. Explicit expressions for these orbits may be found in Appendix A.

Of these, the heteroclinic orbits play the most important part. Due to the shape of $U(R; \mu, L)$ such orbits necessarily involve the trivial state $R = 0$ and require the conditions $E = L = 0$. In addition, we require that the potential $U(R; \mu, 0)$ has a pair of local maxima, one at $R = 0$ and one at $R = R_M \neq 0$, both of the same height. This condition defines the equivalent of a Maxwell point for the present system, $\mu_M = \frac{b^2}{16\beta} < 0$, and requires $b > 0$, $\beta < 0$. The resulting heteroclinic orbit connects the trivial state $R = 0$ to a periodic wave train with $R_M^2 = -\frac{b}{4\beta}$ and $k_M = \frac{(a_1 + a_2)b}{16\beta}$ and, hence, corresponds to a front between the trivial state and a spatially periodic pattern (see Fig. 7 and Appendix A). Note that $k_M \neq 0$ whenever $a_1 + a_2 \neq 0$. One can check that $\mu_{sn}(k_M) \leq \mu_M < 0$ with equality when

$$a_2(a_1 + a_2) = 4. \quad (18)$$

It follows that if $a_2(a_1 + a_2) < 4$, then the amplitude R_M belongs to the $R_0^+(k_M)$ branch and is then referred to as R_M^+ ; if $a_2(a_1 + a_2) > 4$, the amplitude R_M belongs to the

$R_0^-(k_M)$ branch and is then referred to as R_M^- . Since R_0^+ is amplitude-stable while R_0^- is amplitude-unstable it follows that in the former case the front connects two stable states, while in the latter case it connects a stable state ($A = 0$) to an unstable state (A^-). This distinction is of great consequence for the stability and motion of the front. The curve (18) is also shown in Fig. 4.

In Fig. 8, we show for comparison two different homoclinic orbits, the first homoclinic to the trivial state ($A = 0$) and the second to a nontrivial state ($A \neq 0$).

IV. STEADY-STATE BIFURCATIONS FROM PRIMARY BRANCHES

From the discussion in Sec. III, we know that quasiperiodic solutions can bifurcate from the primary branch with fixed wave number k when the equilibrium point corresponding to the amplitude $R_0(k)$ is elliptic. The period of the associated amplitude modulation is approximately equal to $2\pi\sqrt{2/U_{RR}}$ near the original periodic state. If the domain size is finite, boundary conditions select a discrete set of branches from the continuous family of such solutions parametrized by the constants of integration E and L . Since solutions satisfying Neumann boundary conditions (NBC) on a domain of length Γ satisfy periodic boundary conditions (PBC) on a periodic

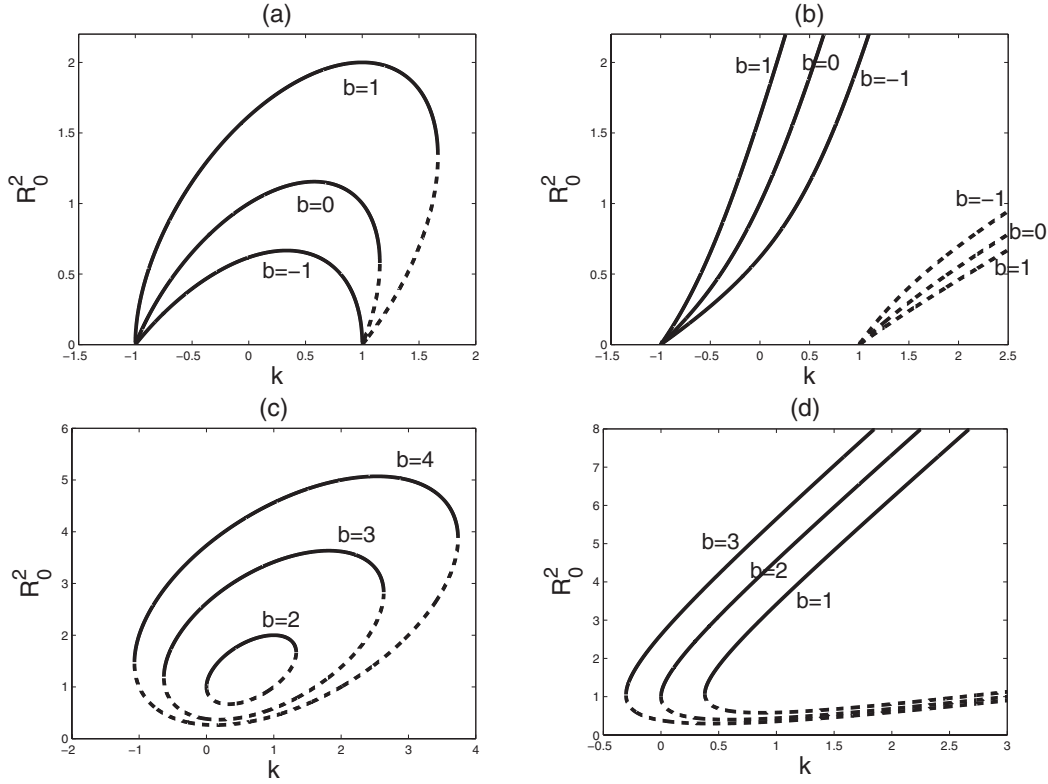


FIG. 3. Bifurcation diagrams showing R_0^2 as a function of k when (a) $\mu = 1, a_2 - a_1 = 1$, (b) $\mu = 1, a_2 - a_1 = 3$, (c) $\mu = -1, a_2 - a_1 = 1$, and (d) $\mu = -1, a_2 - a_1 = 3$. Solid (dashed) lines indicate solutions that are stable (unstable) in time with respect to amplitude perturbations.

domain of period 2Γ , we focus in the following on stationary solutions satisfying NBC at $x = 0, \Gamma$:

$$R_x = 0, \quad \sin \phi = 0. \quad (19)$$

We mention that more generally periodic boundary conditions on $u(x)$, i.e., $u(x + 2\Gamma) = u(x)$ for all x , imply the boundary condition

$$A[\epsilon^2(x + 2\Gamma)] \exp 2ik_c\Gamma = A(\epsilon^2x), \quad (20)$$

for all x on the amplitude A .

In the following we plot bifurcation diagrams showing the solution amplitude measured by the quantity $\| \cdot \|_{H_1}$ as a function of the parameter μ , where

$$\|A\|_{H_1} \equiv \left(\frac{1}{\Gamma} \int_0^\Gamma |A_x|^2 + |A|^2 dx \right)^{1/2}. \quad (21)$$

A. Bifurcations from the $k = 0$ primary branch

Since the $k = 0$ branch is the first of the (subcritical) primary branches to set in for $b > 0$ as μ increases, we present in Figs. 9–15 the $k = 0$ branch together with a number of secondary branches, computed using the continuation software AUTO [28]. These consist of states with spatially varying amplitude $R(x)$ and phase $\phi(x)$ and bifurcate from the $k = 0$

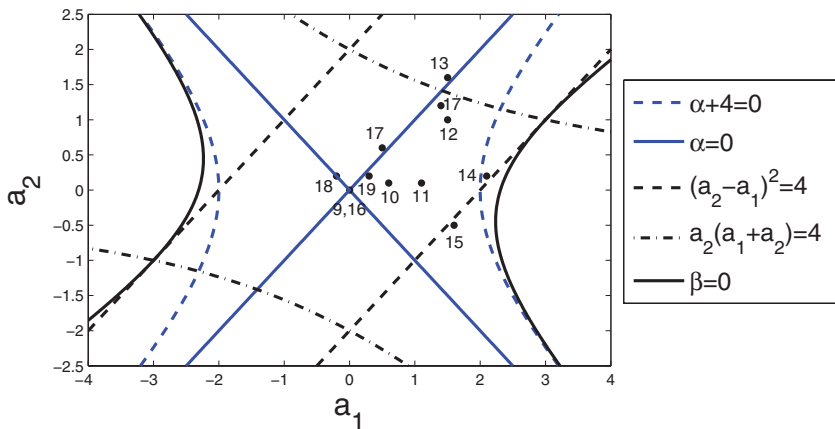


FIG. 4. (Color online) The (a_1, a_2) plane splits into a number of regions with different behavior (see text). Black dots indicate the parameter values used in subsequent figures, with the numbers indicating the corresponding figure. The region $\beta \equiv \frac{(a_1+a_2)^2}{16} - \frac{a_2(a_1+a_2)}{6} - \frac{1}{3} < 0$ (between solid black lines) contains heteroclinic solutions between the origin and either R_0^+ [if $a_2(a_1 + a_2) < 4$] or R_0^- [if $a_2(a_1 + a_2) > 4$]. The line $\alpha \equiv a_2^2 - a_1^2 = 0$ plays a role in determining the sequence of secondary bifurcations (Sec. IV) while the sign of $\alpha + 4$ plays an important role in the temporal analysis (Sec. V).

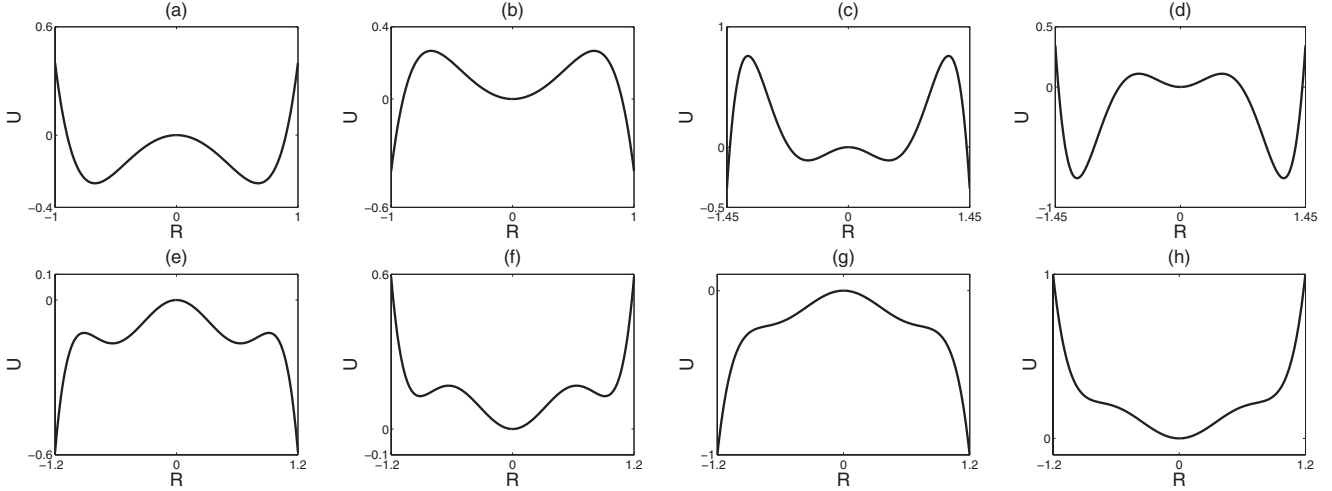


FIG. 5. The potential $U(R; \mu, L)$ when $L = 0$, drawn reflected in $R = 0$. (a) $\mu = -1, b = 1, \beta = 0.9$ ($\mu < 0, \beta > 0$). (b) $\mu = 1, b = -1, \beta = -0.9$ ($\mu > 0, \beta < 0$). (c) $\mu = -1, b = 5, \beta = -1$ ($\mu, \beta < 0$ and $b > 4\sqrt{\mu\beta}$). (d) $\mu = 1, b = -5, \beta = 1$ ($\mu, \beta > 0$ and $b < -4\sqrt{\mu\beta}$). (e) $\mu = -1, b = 3.7, \beta = -1$ ($\mu, \beta < 0$ and $2\sqrt{3\mu\beta} < b < 4\sqrt{\mu\beta}$). (f) $\mu = 1, b = -3.7, \beta = 1$ ($\mu, \beta > 0$ and $-4\sqrt{\mu\beta} < b < -2\sqrt{3\mu\beta}$). (g) $\mu = -1, b = 3.3, \beta = -1$ ($\mu, \beta < 0$ and $b < 2\sqrt{3\mu\beta}$). (h) $\mu = 1, b = -3.3, \beta = 1$ ($\mu, \beta > 0$ and $b > -2\sqrt{3\mu\beta}$).

branch in secondary bifurcations we refer to as Eckhaus bifurcations (see Sec. V). These secondary branches either terminate on the same $k = 0$ branch or do so on a different primary branch ($k \neq 0$) or not at all. Figure 9 reveals that when $a_1 = a_2 = 0$ [29,30] the secondary branches originate and terminate on the same $k = 0$ primary branch. Each branch can be labeled by a pair of integers (n, m) specifying the number of half wavelengths of $R(x)$ and $\phi(x)$ within the domain Γ . Solutions with $n = 1$ (the first secondary branch) bifurcate nearest to the primary bifurcation at $\mu = 0$ and terminate nearest to the saddle node. Figure 10(a) shows typical results when $a_1 a_2 \neq 0$. In this case, unless b is too small [Fig. 10(b)], the $n = 1$ branch no longer terminates on the $k = 0$ primary branch but terminates instead on the primary branch with $k = \pi/\Gamma$. However, since an $n = 1$ Eckhaus instability near the $k = 0$ saddle node remains, a new $n = 1$ branch bifurcates from the $k = 0$ branch near the saddle-node bifurcation and this time extends monotonically to larger amplitudes. States of this type represent a defect in the original wave train with wave number k_c that may be located either in the center of the domain or at its boundary, e.g., Fig. 12(b), and we refer to them as defect states [7]. These states

resemble those familiar from studies of the Eckhaus instability for supercritical Ginzburg-Landau equation [12,13] but are present here even for $k = 0$. The figures show that the defect states bifurcate from the $k = 0$ branch either below or above the saddle node, depending on parameters; for increasingly negative b the bifurcation point moves to larger and larger amplitude, leaving behind stable supercritical periodic states. The termination points of the smaller amplitude secondary branches may likewise lie below or above the saddle node. Figures 11–13 show that these basic effects of the presence of the coefficients a_1, a_2 persist to other values provided $a_1^2 - a_2^2 - 4 < 0$ [see Eq. (14) with $k = 0$]. In contrast, when $a_1^2 - a_2^2 - 4 > 0$ (Figs. 14 and 15) the secondary branches are all strongly subcritical and all terminate on branches with $k \neq 0$. The curves $a_1^2 - a_2^2 - 4 = 0$ are also shown in Fig. 4.

It will have been noticed that all secondary branches bifurcating from R_0^- , except those bifurcating close to the saddle node, develop a protosnaking region with a sudden increase of H_1 norm located near the Maxwell point $\mu_M = \frac{b^2}{16\beta} < 0$. This point plays a fundamental role in understanding the behavior shown in Figs. 9–15. We have seen that at $\mu = \mu_M$, a heteroclinic connection between

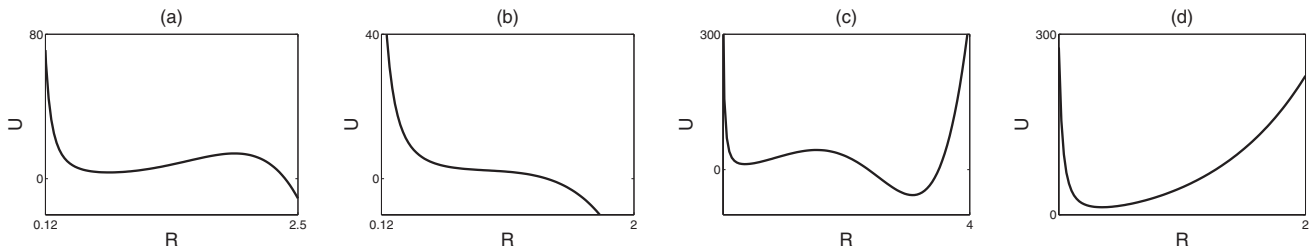


FIG. 6. The potential $U(R; \mu, L)$ when $L = 1$. (a) $\mu = 1, b = 4, a_1 = 1, a_2 = 1$ [$\beta < 0, R_{0,+}^2 > 0, R_{0,-}^4(\mu' + bR_{0,-}^2/2) > 2L^2$]. (b) $\mu = 1, b = -1, a_1 = 1, a_2 = 1$, [$\beta < 0$ and at least one of the other conditions in (a) is violated]. (c) $\mu = 40, b = -20, a_1 = 4, a_2 = 0.5$ [$\beta > 0, b < 0, 0 < 32\beta\mu' < 3b^2, R_{0,+}^4(\mu' + bR_{0,+}^2/2) < 2L^2$]. (d) $\mu = 40, b = 5, a_1 = 4, a_2 = 0.5$ [$\beta > 0$ and at least one of the other conditions in (c) is violated]. Here $\mu' \equiv \mu + \frac{3a_2 - a_1}{2}L$ and $R_{0,\pm}^2 \equiv \frac{-b \pm \sqrt{b^2 - 32\beta\mu'/3}}{8\beta}$.

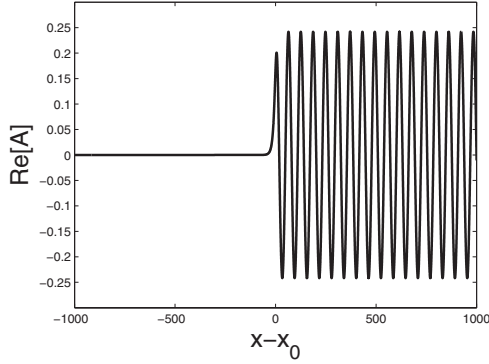


FIG. 7. The profile $\text{Re}A(x)$ from Appendix A, Eq. (A1), of the heteroclinic solution at $\mu = \mu_M \approx -0.0146$ when $b = 1$, $a_1 = 1$, and $a_2 = 6$.

$A = 0$ and $A = R_M \exp ik_M x$ is present (Fig. 7). Although one might expect the presence of homoclinic snaking extending over a finite interval whenever $k_M \neq 0$, this is not the case here due to the absence of a coupling between the front and the spatial oscillations with wave number k_M . As a result the snaking region collapses to a single point $\mu = \mu_M$. Despite this, the presence of this point determines the branch on which the secondary branches involved terminate. This is because the presence of the heteroclinic orbit at $\mu = \mu_M$ determines the wave number k_M , and this wave number in turn determines the primary branch on which the branches terminate. For example, in Fig. 9, the selected wave number $k_M = 0$ and all secondary branches terminate on the $k = 0$ branch from which they first bifurcated. In Fig. 10, the wave number $k_M \approx -0.0696$ and indeed the $n = 1$ branch no longer terminates on a $k = 0$ branch and instead terminates on a primary branch with wave number closest to k_M that is compatible with the imposed NBC and domain length Γ , viz. $|k| = \pi/\Gamma = 0.0625$ ($m = 1$). The secondary branches with $n \geq 2$ do not come sufficiently close to forming the heteroclinic orbit and so continue to terminate on the $k = 0$ branch. In Figs. 11 and 12 the corresponding wave numbers are $k_M = -0.1424$ ($m = 2$) and $k_M = -0.2174$ ($m = 3$) and these wave numbers determine the type of change that must take place before the different secondary solutions can

approach the heteroclinic connection. These changes are illustrated clearly in the lower panels in Fig. 11 which show that the branches bifurcating at points 1 ($n = 1$) and 2 ($n = 2$) both become $m = 2$ states despite bifurcating at different locations from the $k = 0$ branch. Since phase has to be added along these secondary branches for these changes to take place it follows that the quantity L in the potential $U(R; \mu, L)$ must either pass through zero in order that the phase may jump by π or remain identically zero so multiple phase changes can take place.

In Figs. 9–12 the heteroclinic orbit that forms at μ_M connects the states $R = 0$ and R_M^+ . In Fig. 13 it connects instead the states $R = 0$ and R_M^- , i.e., a stable state $R = 0$ to an amplitude-unstable state R_M^- . In such a situation the associated front will move, allowing the stable state to invade the unstable state. For the cases $a_1^2 - a_2^2 - 4 > 0$ with $(a_1 - a_2)^2 - 4 < 0$ (Fig. 14) and $a_1^2 - a_2^2 - 4 < 0$ with $(a_1 - a_2)^2 - 4 > 0$ (Fig. 15), the predictions $\mu_M \approx -0.197$, $R_M^+ \approx 1.255$, $k_M \approx -0.906$ (Fig. 14) and $\mu_M \approx -0.0941$, $R_M^+ \approx 0.8677$, $k_M \approx -0.207$ (Fig. 15) continue to agree well with the numerical computations shown in the figures. Thus, the wave-number selection process via the formation of a heteroclinic connection continues to determine the termination points of the secondary branches even when the $k \neq 0$ primary branches are highly subcritical.

The above bifurcation diagrams have all been obtained for a domain of one given length, $\Gamma = 16\pi$. When Γ is increased, the termination points of the secondary branches must switch to branches containing extra wavelengths of the Maxwell wavelength $\lambda_M = 2\pi/k_M$. The mechanism whereby this occurs has been studied in detail in gradient systems, such as the 2–3 and 3–5 Swift-Hohenberg equations [7,30], and is relatively well understood. Similar behavior has also been found in nongradient systems such as the partial differential equations describing natural doubly diffusive convection [7]. For these reasons we do not study the details of these transitions in this paper.

B. Bifurcations from the $k = 1$ primary branch

In Figs. 16 and 17 we show the corresponding results for the primary $k = 1$ bifurcation. As shown in Appendix B, when

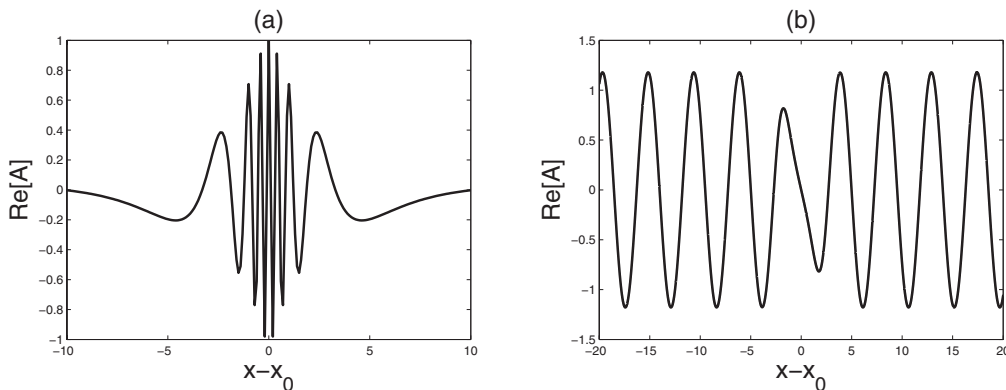


FIG. 8. (a) Homoclinic solution to $A = 0$ at $\mu = 0$ when $b = -2$, $\beta = 1$, and $a_1 + a_2 = 64$ [Appendix A, Eq. (A5)]. (b) Homoclinic solution to a nonzero equilibrium corresponding to a rotating wave at $\mu = -1$ with $R_0 \approx 1.1791$ and $k = -1.3903$ when $b = 3.5$, $a_1 = a_2 = 2$ [Appendix A, Eq. (A6)].

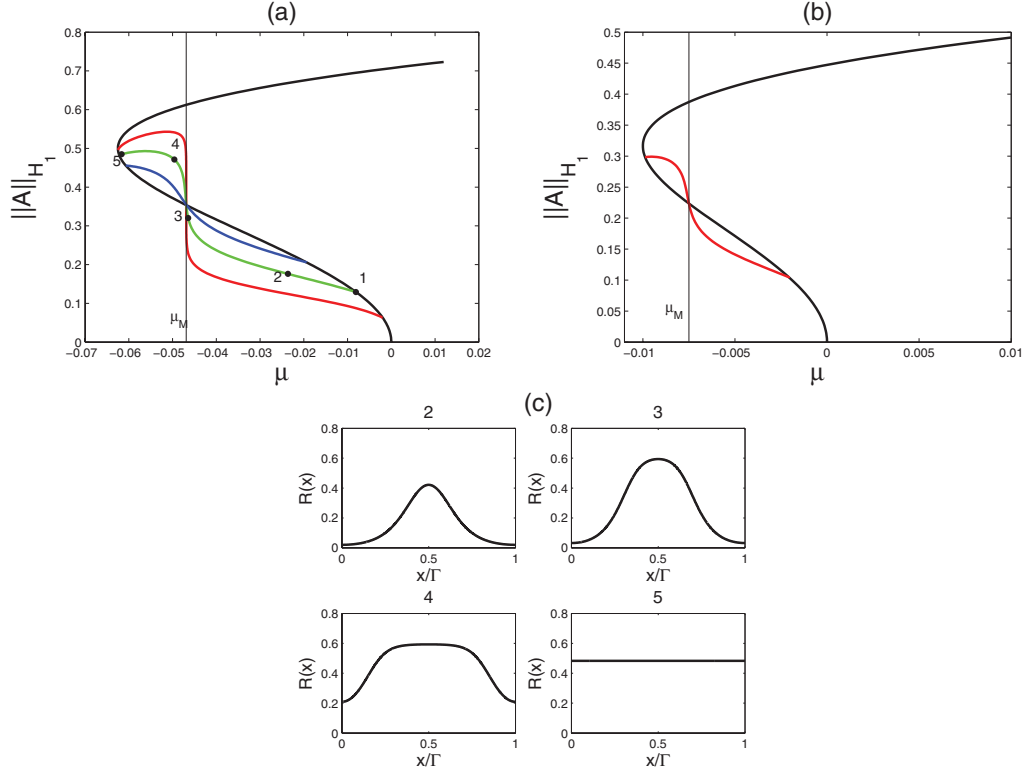


FIG. 9. (Color online) Bifurcation diagrams for subcritical stationary solutions with $k = 0$ with several secondary branches of nonuniform states satisfying NBC. Parameters: $a_1 = 0$, $a_2 = 0$, $\Gamma = 16\pi$. (a) $b = 0.5$. (b) $b = 0.2$. (c) Sample profiles $R(x)$ along the branch bifurcating from point 1 in (a).

$a_1 = a_2 = 0$ two steady-state branches bifurcate together from $\mu = 1$. The prediction follows from a careful analysis of the symmetry of the problem when periodic boundary conditions are imposed and is confirmed in Fig. 16. The larger amplitude branch consists of RW states of the form $A = R_0 \exp i(x + \phi_0)$, where R_0 is a constant, while the smaller amplitude branch consists of SW states of the form $A = R(x) \exp i\phi_0$, where $R(x)$ is x dependent and near $\mu = 1$ resembles $\cos x$. Here ϕ_0 is an arbitrary phase. Both states, of course, satisfy periodic boundary conditions in space and can be translated in x to satisfy the imposed NBC. Figure 16(a) also shows that the RW and SW branches may be connected by a secondary branch of time-independent states, of the form $A = R(x) \exp i(\phi(x) + \phi_0)$, while other secondary branches bifurcating from the RW branch develop into defect states and extend monotonically to large amplitude [Fig. 16(d)]. Figure 16 shows that the former are periodic since both $R(x)$ and $\phi(x)$ oscillate with same frequency, while along the latter $R(x)$ and $\phi(x)$ oscillate with different frequencies and the solutions appear quasiperiodic.

Once either a_1 or a_2 is nonzero, a similar analysis shows that the RW branch splits into two distinct rotating waves RW^\pm , both of which continue to bifurcate simultaneously from $\mu = 1$. In addition, when $0 < |k(a_1 + a_2)| < |b|$ the SW state turns into a mixed mode (MW) state that bifurcates from the $A = 0$ state simultaneously with the RW^\pm . The MW are no longer present as a primary branch once $|k(a_1 + a_2)| > |b|$ (see Appendix B). Figure 17(a) shows the RW^\pm in the subcritical case when $a_1 = 0.6$, $a_2 = 0.8$, $b = 0.5$. Thus, in this case no MW are present as a primary branch although the figure

reveals the presence of two types of finite-amplitude secondary branches resembling states of this type. The first type bifurcates from the $k = 1$ RW^+ branch below the saddle node and terminates on a primary branch with $k \neq 0, 1$. The second type represents defect states that extend to large amplitudes without termination. These secondary branches are outside of the range of validity of the weakly nonlinear theory in Appendix B but are found in a higher codimension analysis of the $a_1 = a_2 = 0$ degeneracy [31]. Only the defect states are present in the supercritical case [Fig. 17(b), $a_1 = 1.4$, $a_2 = 1.2$, $b = -0.5$].

In the special case $a_1 + a_2 = 0$ the MW states degenerate into SW and bifurcate from $\mu = 1$ together with the RW^\pm . Figure 18 shows an example of the resulting bifurcation diagram. Finally, Fig. 19 shows an example with $0 < |k(a_1 + a_2)| < |b|$ in which the MW are present and bifurcate together with the RW^\pm . However, at larger amplitudes the two sets of branches differ substantially in their behavior, with the MW terminating on RW^- .

C. Infinite domains and quasiperiodic wave trains

We have seen that when $k = 1$ either one or two branches of periodic states bifurcate from $\mu = 1$ depending on the coefficients a_1 and a_2 . In contrast, when $k = 0$ there is only one branch of equilibria, and it bifurcates at $\mu = 0$. On an infinite domain we may look for solutions with a small but nonzero wave number. When a_1 or a_2 is nonzero, we expect a bifurcation to periodic RW, much as in the preceding section. However, the SW become quasiperiodic states as we now

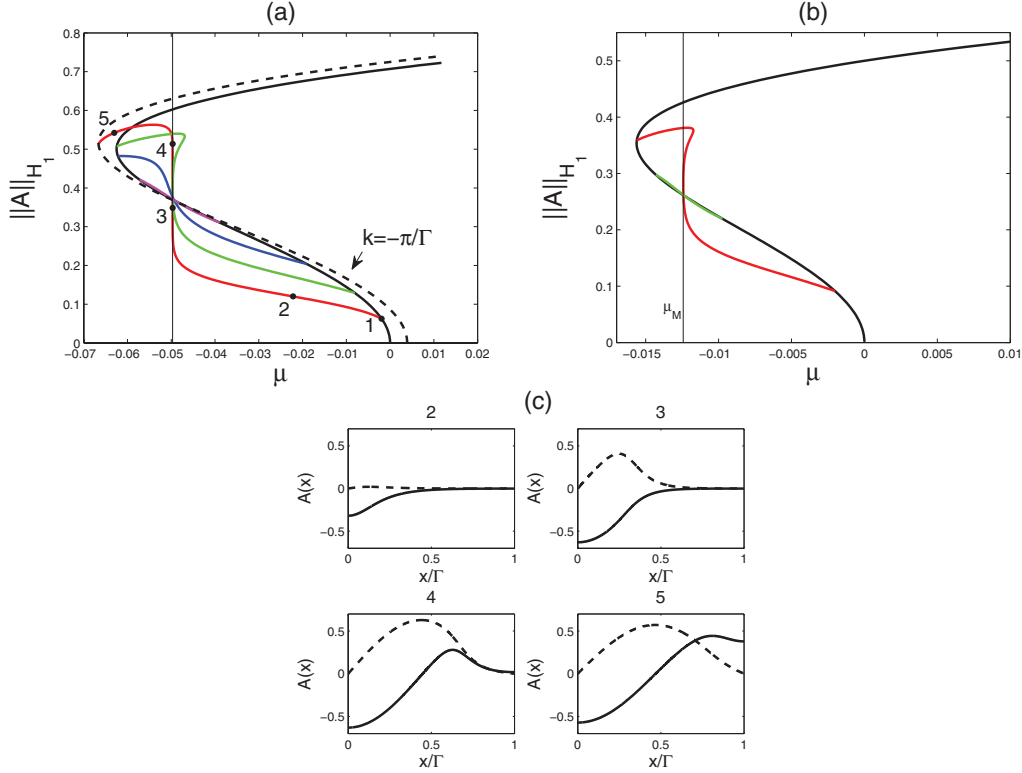


FIG. 10. (Color online) Bifurcation diagrams for subcritical stationary solutions with $k = 0$ with several secondary branches of nonuniform states satisfying NBC. Parameters: $a_1 = 0.6$, $a_2 = 0.1$, $\Gamma = 16\pi$. (a) $b = 0.5$. (b) $b = 0.25$. (c) Sample profiles of $\text{Re}A(x)$ (solid line) and $\text{Im}A(x)$ (dashed line) along the branch bifurcating from point 1 in (a). This branch terminates on a primary branch with $k = -\pi/\Gamma \approx k_M$.

demonstrate using formal perturbation theory. We suppose that $\mu = O(\epsilon^2)$, where $\epsilon \ll 1$. The RW take the form

$$A = \epsilon R_0 \exp ikx + O(\epsilon^2), \quad (22)$$

where $k = O(\epsilon)$, while the quasiperiodic states take the different form

$$A = \epsilon R(X, \epsilon) \exp i\epsilon\phi(X, \epsilon) + O(\epsilon^2), \quad (23)$$

where $X \equiv \epsilon x$ is a slow spatial scale. Substituting this ansatz into Eq. (7) with $R(X, \epsilon) = R_0(X) + \epsilon R_1(X) + \dots$, $\phi(X, \epsilon) = \phi_0(X) + \epsilon\phi_1(X) + \dots$, $\mu = \epsilon^2\mu_2$, we obtain at $O(\epsilon^3)$

$$R_{0XX} + \mu_2 R_0 + bR_0^3 = 0 \quad (24)$$

and at $O(\epsilon^4)$

$$\phi_{0X} = -\frac{1}{4}(a_1 + a_2)R_0^2 \neq 0. \quad (25)$$

Thus, rotating waves and quasiperiodic states bifurcate simultaneously from $A = 0$ at $\mu = 0$, much as in the Swift-Hohenberg equation [6]. However, due to the absence of pinning, there is a one-parameter family of quasiperiodic solutions, parametrized by an arbitrary phase. In finite domains, however large, the quasiperiodic solutions are expected to bifurcate from the RW at small but finite amplitude.

D. Theoretical interpretation

It is possible to develop, to a certain extent, a theoretical understanding of the above results. The understanding is based on the presence of the conserved quantities E and L

and the shape of the potential $U(R; \mu, L)$ [Eqs. (10)–(13)]. With NBC, i.e., $R_x = 0$ at $x = 0, \Gamma$, secondary bifurcations to two-frequency states can only occur on a primary branch at locations where

$$U_{RR} = \frac{2\pi^2 n^2}{\Gamma^2}, \quad n \in \mathbb{N}. \quad (26)$$

Explicit expression for U_{RR} can be found in Eq. (14). Since stationary solutions are determined up to translation in x and phase rotation by the integrals E and L , the behavior of a branch of two-frequency states is determined by a set of implicit functions containing E and L with μ as a bifurcation parameter. These relations capture the requirement that an integer number of half-wavelengths of both $R(x)$ and $\phi(x)$ fit in the domain Γ and take the form

$$\frac{\Gamma}{n} = \int_{R_{\min}}^{R_{\max}} \frac{dR}{R_x} = \int_{R_{\min}}^{R_{\max}} \frac{dR}{\sqrt{E - U(R; \mu, L)}}, \quad n \in \mathbb{N}, \quad (27)$$

$$\frac{m\pi}{n} = \int_{R_{\min}}^{R_{\max}} \frac{\phi_x dR}{R_x} = \int_{R_{\min}}^{R_{\max}} \frac{L/R^2 - \frac{a_1 + a_2}{4} R^2}{\sqrt{E - U(R; \mu, L)}} dR, \quad m \in \mathbb{Z}. \quad (28)$$

Here R_{\min} and R_{\max} are the roots of $E = U(R; \mu, L)$ corresponding to the turning points of the trajectory in the potential. Thus each branch of two-frequency states is determined by a pair of integers n and m . In particular, on the primary $k = 0$ branch, the secondary bifurcation points satisfy, cf., Eq. (14)

$$U_{RR} = 4bR_0^2 + 2(a_1^2 - a_2^2 - 4)R_0^4 = 2\pi^2 n^2 / \Gamma^2, \quad (29)$$

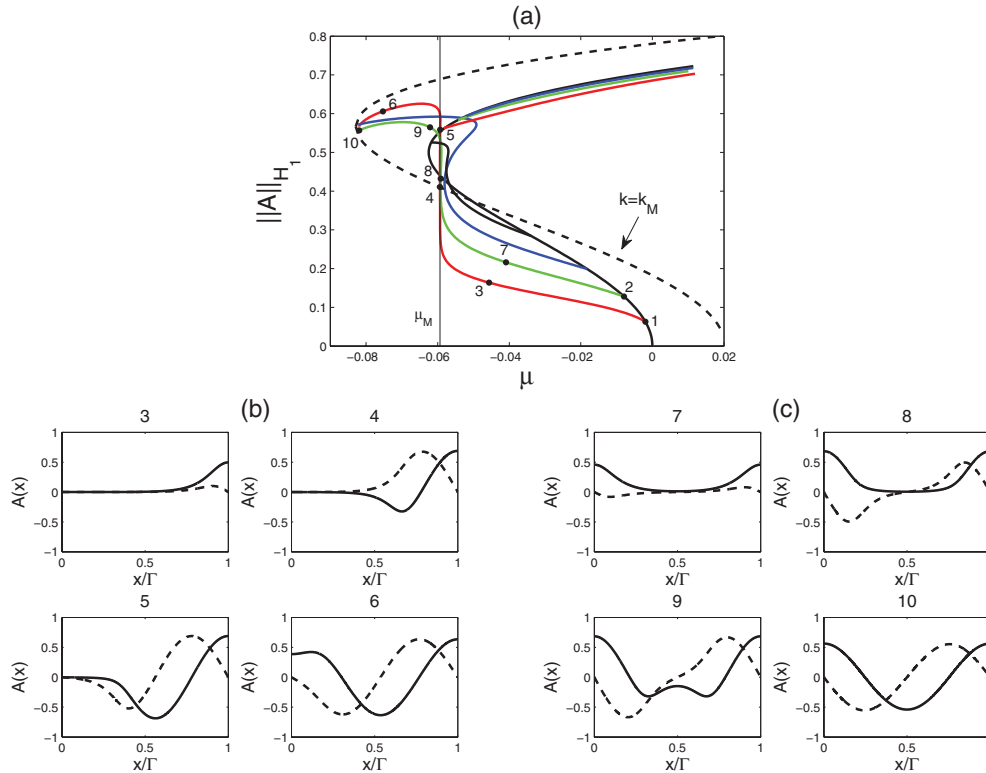


FIG. 11. (Color online) (a) Bifurcation diagram for subcritical stationary solutions with $k = 0$ with several secondary branches of nonuniform states satisfying NBC. The first three secondary branches terminate on a primary branch with $k \neq 0$. [(b) and (c)] Sample profiles of $\text{Re}A(x)$ (solid line) and $\text{Im}A(x)$ (dashed line) along the branch bifurcating from points 1 and 2, respectively, showing that both branches terminate on a primary branch with wave number $k = -2\pi/\Gamma \approx k_M$. Parameters: $b = 0.5, a_1 = 1.1, a_2 = 0.1, \Gamma = 16\pi$.

cf. Eq. (14). Thus, in the supercritical case ($b < 0$), $U_{RR} < 0$ when $a_1^2 - a_2^2 - 4 \leq 0$ and no secondary bifurcations are present. However, if $a_1^2 - a_2^2 - 4 > 0$ the quantity U_{RR} becomes positive at sufficiently large R , triggering secondary bifurcations. In contrast, in the subcritical case ($b > 0$) U_{RR} increases monotonically with R_0 provided $a_1^2 - a_2^2 - 4 \geq 0$, and, consequently, secondary bifurcations for each n appear exactly once

along the branch. However, when $a_1^2 - a_2^2 - 4 < 0$ U_{RR} first increases with R_0 but then decreases. When $a_2^2 - a_1^2 = 0$, $U_{RR} \geq 0$ along the whole R_0^- branch; if $-4 < a_2^2 - a_1^2 < 0$ the region where $U_{RR} \geq 0$ extends above the saddle node, but it shrinks below the saddle node if $a_2^2 - a_1^2 > 0$. If $a_2^2 - a_1^2$ is so large that the maximum of U_{RR} falls below π^2/Γ^2 , no bifurcation point is present. These results are reflected in the properties of Figs. 9–15. In the case

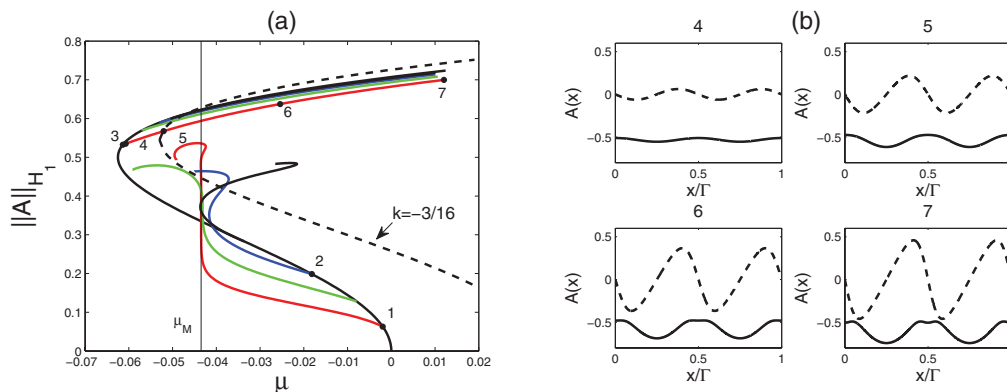


FIG. 12. (Color online) (a) Bifurcation diagram for subcritical stationary solutions with $k = 0$ with several secondary branches of nonuniform states satisfying NBC. Parameters: $b = 0.5, a_1 = 1.5, a_2 = 1.0, \Gamma = 16\pi$. Branches bifurcating at points 1 and 2 in (a) terminate at the same wave number, $k = -3/16$. (b) Sample profiles of $\text{Re}A(x)$ (solid line) and $\text{Im}A(x)$ (dashed line) along the defect branch bifurcating at point 3 in (a).

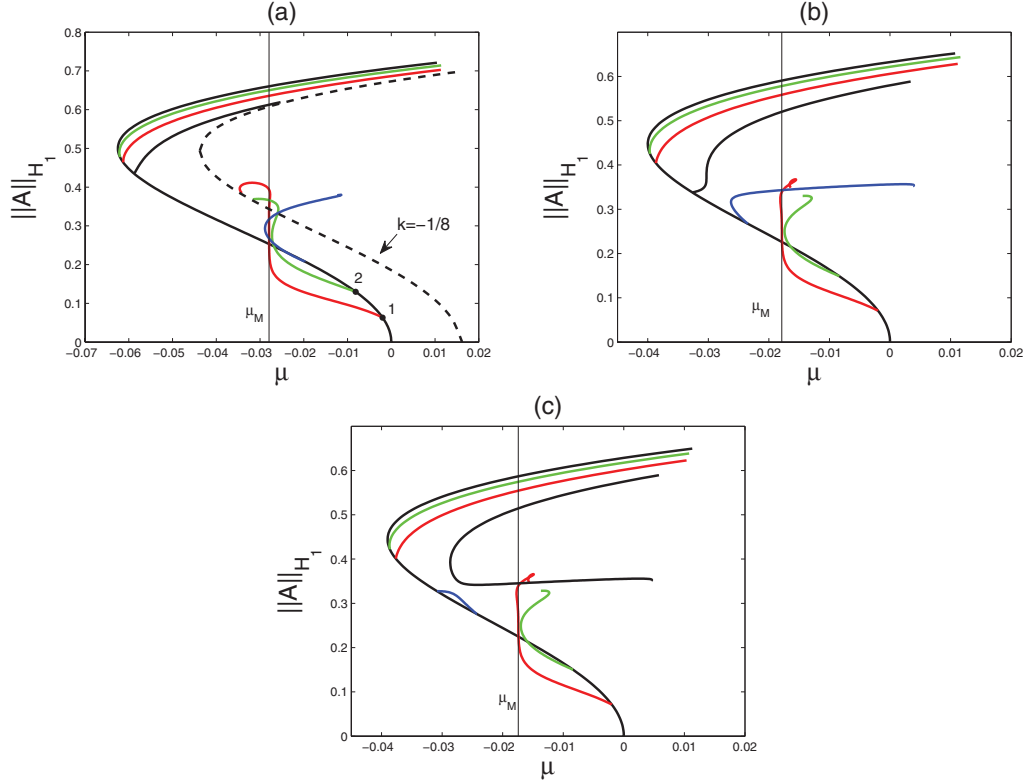


FIG. 13. (Color online) Bifurcation diagrams for subcritical stationary solutions with $k = 0$ with several secondary branches of nonuniform states satisfying NBC showing the reconnection process that takes place with decreasing b . Branches bifurcating at points 1 and 2 in (a) terminate at the same wave number, $k = -1/8$. Parameters: $a_1 = 1.5$, $a_2 = 1.6$, $\Gamma = 16\pi$. (a) $b = 0.5$. (b) $b = 0.4$. (c) $b = 0.395$.

$a_1^2 - a_2^2 < 4$, if we increase the domain size Γ , the number of bifurcation points scales as Γ . The bifurcation points accumulate near $U_{RR} = 0$, i.e., at $R_0^2 = 0$ and $R_0^2 = \frac{2b}{4+a_2^2-a_1^2}$. If we let μ_n be the n th bifurcation point in the sequence that accumulates at $R_0 = 0$ when Γ is large (i.e., at $\mu = 0$), then the μ_n scale as n^2/Γ^2 and a similar scaling holds at the other accumulation point unless this point coincides with the saddle node. In the latter case $a_1^2 = a_2^2$ and the distance $\delta\mu_n$ from the saddle node scales as n^4/Γ^4 . Note that since the integer n represents the mode number, the accumulation point is reached in the limit $n \rightarrow 1$, with n/Γ , $n = 1$, representing the smallest wave number allowed by the boundary conditions. Such scaling laws are also found in the Swift-Hohenberg equation and arise in studies of natural doubly diffusive convection as well [7]. As shown in Appendix C, the direction of branching of the resulting quasiperiodic states is readily computable and the predictions therein agree well with our numerical computations.

When $k \neq 0$ the conditions (28) provide implicit relations that determine the locations of bifurcation points. The integrals can be evaluated in terms of Jacobi elliptic functions, and the results determine the variation of E and L with the parameter μ along the secondary branch. Each branch is characterized by the integer n , which is constant along the branch. This is not true for the integer m , however, which is, in general, only piecewise constant along the branch. This is a consequence of phase jumps that may take place along the branch. These occur when R passes through zero at some $x \in (0, \Gamma)$

and require that simultaneously $L = 0$. The phase jump is determined by writing

$$\int_{R_{\min}}^{R_{\max}} \frac{LdR}{R^2\sqrt{E-U}} = \int_{R_{\min}}^{R_*} \frac{LdR}{R^2\sqrt{E-U}} + \int_{R_*}^{R_{\max}} \frac{LdR}{R^2\sqrt{E-U}} \quad (30)$$

and taking $R_* = O(|L|^p)$, $1/2 < p < 1$. The integral from R_* to R_{\max} [$=O(1)$] is $O(|L|/R_*)$ and so vanishes in the limit $L \rightarrow 0$. The first integral dominates because $R_{\min} = |L|/\sqrt{E} + o(|L|)$ as $L \rightarrow 0$, $E = O(1)$, and $U - L^2/R^2 = O(R^2) = o(L^2/R^2)$ in $R_{\min} < R < R_*$. Thus

$$\lim_{L \rightarrow 0} \int_{R_{\min}}^{R_*} \frac{LdR}{R^2\sqrt{E-U}} = \text{sgn}(L) \int_1^\infty \frac{dr}{r^2\sqrt{1-1/r^2}} = \text{sgn}(L) \frac{\pi}{2}, \quad (31)$$

where $\text{sgn}(L)$ denotes the sign of L along the branch before it reaches 0. Thus, the total change of phase over the domain Γ as L crosses zero is $-\text{sgn}(L)n\pi$. The phase remains constant unless another phase jump takes place. It follows from Eq. (28b) that

$$\int_0^{R_{\max}} \frac{(a_1 + a_2)R^2}{4\sqrt{E-U}} dR = \pi \left[\frac{\text{sgn}(L)}{2} - \frac{m}{n} \right]. \quad (32)$$

This relation constrains greatly the phase jumps that may occur along the secondary branches and, in particular, the allowed

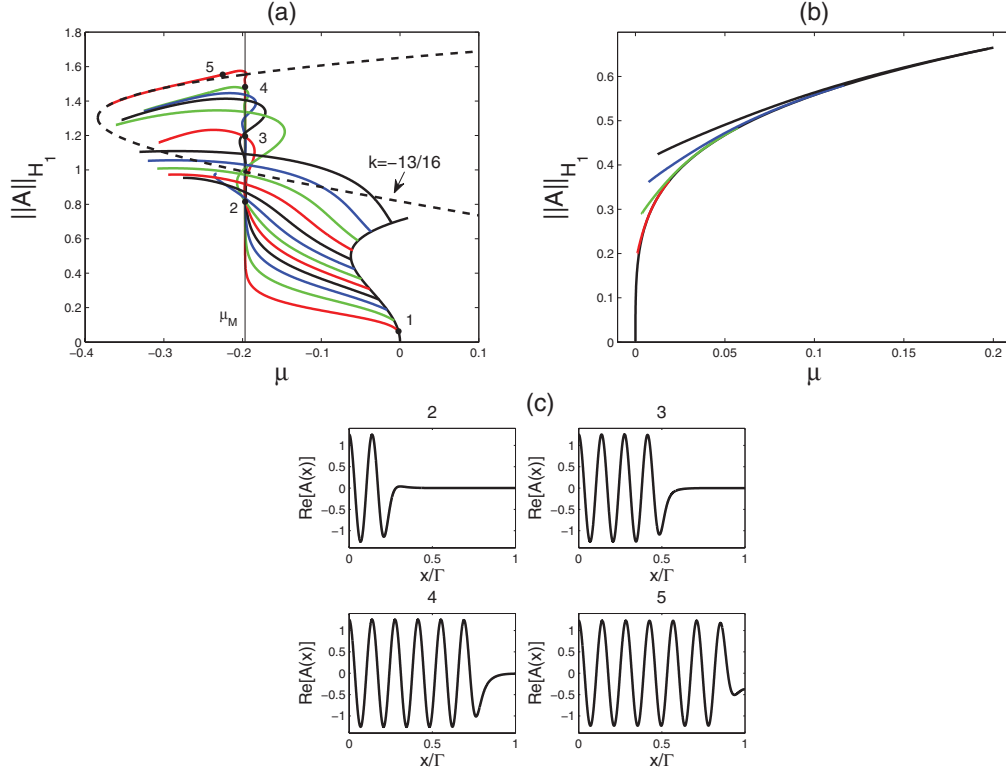


FIG. 14. (Color online) Bifurcation diagrams for (a) subcritical and (b) supercritical stationary solutions with $k = 0$ with several secondary branches of nonuniform states satisfying NBC. All secondary branches terminate at nonzero wave number. Parameters: $a_1 = 2.1$, $a_2 = 0.2$, $\Gamma = 16\pi$. (a) $b = 0.5$. (b) $b = -0.01$. (c) Sample profiles of $\text{Re}A(x)$ along the branch bifurcating from point 1 in (a).

interconnections among the primary branches. In particular, in the special case $a_1 = -a_2$, the necessary condition for a phase jump to take place is $2m = \text{sgn}(L)n$. Thus, if the primary branch has nonzero wave number $k = \frac{m\pi}{\Gamma}$ the condition $U_{RR} = \frac{2\pi^2 n^2}{\Gamma^2}$ for a secondary bifurcation collapses to $bR_0^2 - 2R_0^4 = 0$, implying that the only secondary branch that can undergo a phase jump is the branch bifurcating at $R_0^2 = b/2$. We emphasize that these phase jumps correspond to phase jumps that occur over large scales in the original problem; strictly, we cannot take the limit $L \rightarrow 0$ without encountering higher-order terms omitted from the Ginzburg-Landau description (2).

E. Transition from subcritical to supercritical behavior

The results presented above enable us to understand the sequence of transitions that must take place as b decreases through $b = 0$ and the $k = 0$ primary branch goes from being subcritical to being supercritical. There are two fundamentally distinct scenarios, distinguished by the sign of the quantity $a_1^2 - a_2^2 - 4$. When $a_1^2 - a_2^2 - 4 < 0$ Fig. 9 shows that as b decreases the secondary bifurcation points on the $k = 0$ branch move to a higher amplitude while the termination points move toward a lower amplitude. In addition, since k_M is proportional to b , its magnitude decreases, thereby making it more and more likely that the secondary branch originates and terminates on the same branch. The mechanism whereby the termination point switches from a primary branch with $k \approx k_M$ to the $k = 0$ branch relies on reconnection between the

protosnaking branch and a defect branch originating from the $k = 0$ branch (not shown), as discussed elsewhere [7]. Similar reconnections eliminate the secondary branches one by one until none remain. Figure 13 shows an example of this process: as b decreases an $n = 3$ mixed mode branch approaches and reconnects with a defect branch, leaving behind a short segment connecting the subcritical $k = 0$ branch to itself together with a larger amplitude, completely disconnected branch of defectlike states. With further decrease of b the end points of the short segment come together, eliminating the segment, while the disconnected branch moves farther away. In this particular example the protosnaking branches turn toward larger μ and undergo a twist before terminating on a periodic state but this does not occur in other cases we have examined. Thus, when $a_1^2 - a_2^2 - 4 < 0$ secondary bifurcation points annihilate pairwise and there is a minimum value of b , $b_{\min} \equiv (\pi/\Gamma)\sqrt{4 + a_2^2 - a_1^2}$, such for $0 < b < b_{\min}$ no secondary bifurcations take place on the subcritical branch, i.e., localized states are absent.

Figure 15 shows that similar reconnections are responsible for successive elimination of the secondary branches in the case $a_1^2 - a_2^2 - 4 > 0$ as well. In this case, the secondary branches bifurcate strongly subcritically and the Maxwell point μ_M typically falls outside the coexistence range between $A = 0$ and the $k = 0$ branch [Fig. 14(a)]. As b decreases both μ_M and $\mu_{\text{sn}}(0)$ decrease as b^2 , implying that in large domains secondary branches continue to bifurcate subcritically. Moreover, when b decreases the secondary bifurcation points move

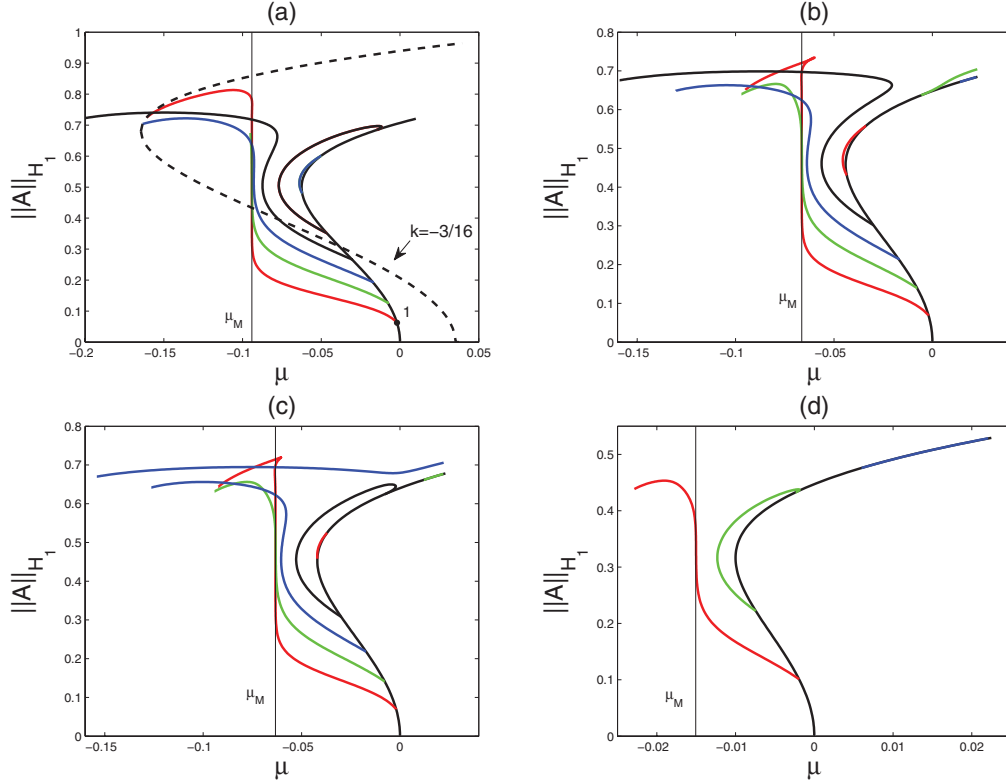


FIG. 15. (Color online) Bifurcation diagrams for subcritical stationary solutions with $k = 0$ with several secondary branches of nonuniform states satisfying NBC. Some secondary branches terminate on the $k = 0$ primary branch. Parameters: $a_1 = 1.6$, $a_2 = -0.5$, $\Gamma = 16\pi$. (a) $b = 0.5$. (b) $b = 0.42$. (c) $b = 0.41$. (d) $b = 0.2$.

up in amplitude and so move through the saddle node to the upper $k = 0$ branch as the saddle node moves downward. Of course, the protosnaking behavior disappears as the system becomes supercritical but the subcritical secondary branches remain [Fig. 14(b)]. These terminate on periodic states that bifurcate subcritically from $A = 0$ at $\mu > 0$, cf. Fig. 2(c).

Figure 16(b) shows a typical result in the supercritical case $b = -0.5$ with $k = 1$ and $a_1 = a_2 = 0$. The two branches that bifurcate from $A = 0$ at $\mu = 1$ are both supercritical and only secondary branches of defect type are present, much as in the standard Eckhaus problem [13]. In contrast, once $a_1 a_2 \neq 0$ [Fig. 17(b)] the SW branch is absent and additional Eckhaus bifurcations occur on the RW branch at small amplitude with connections to primary branches with $k \neq 0, 1$, while defect states continue to bifurcate at larger amplitudes. Observe that no protosnaking develops on any of the secondary branches bifurcating from the $k = 1$ branches, implying the absence of heteroclinic connections between $A = 0$ and $A = R_0 \exp ix$. This is a consequence of the centrifugal barrier ($L \neq 0$) in the potential $U(R; \mu, L)$ for this state and is, in turn, a consequence of the fact that here $k = 1$ is selected by the boundary conditions and not by the condition for a heteroclinic connection.

V. TEMPORAL STABILITY ANALYSIS

In this section we examine the stability properties of primary branches with both $k = 0$ and $k \neq 0$ with respect to long-wave perturbations with wave number $|q| \ll |k|$. The

analysis performed is analogous to the classical Eckhaus analysis [11] but the results, presented in the form of stability regions in the (k, μ) plane, substantially differ due to the subcriticality of the basic wave train and the presence of the coefficients a_1, a_2 , assumed to be nonzero. The problem is formally posed on the real line and no boundary conditions are imposed on the perturbations.

A. Stability of primary branches

Nontrivial constant-amplitude steady solutions $A = R_0 \exp i(kx + \phi_0)$ of Eq. (2) fall into three classes:

(1) Supercritical case: $b' \leq 0$, R_0^+ exists in the region $\mu > k^2$.

(2) Subcritical case: $b' > 0$, R_0^+ solution exists in the region $\mu \geq k^2 - \frac{b^2}{4}$.

(3) Subcritical case: $b' > 0$, R_0^- solution exists in the region $k^2 - \frac{b^2}{4} < \mu < k^2$.

To study the stability, we calculate the spectrum of periodic solutions by writing

$$A = R_0 e^{i(kx + \phi_0)} (1 + a). \quad (33)$$

The perturbation $a \equiv a(x, t)$ evolves according to

$$a_t = -(2\mu - 2k^2 + b'R_0^2)(a + a^*) + 2ika_x + a_{xx} + iR_0^2(a_1 a_x + a_2 a_x^*) + O(|a|^2). \quad (34)$$

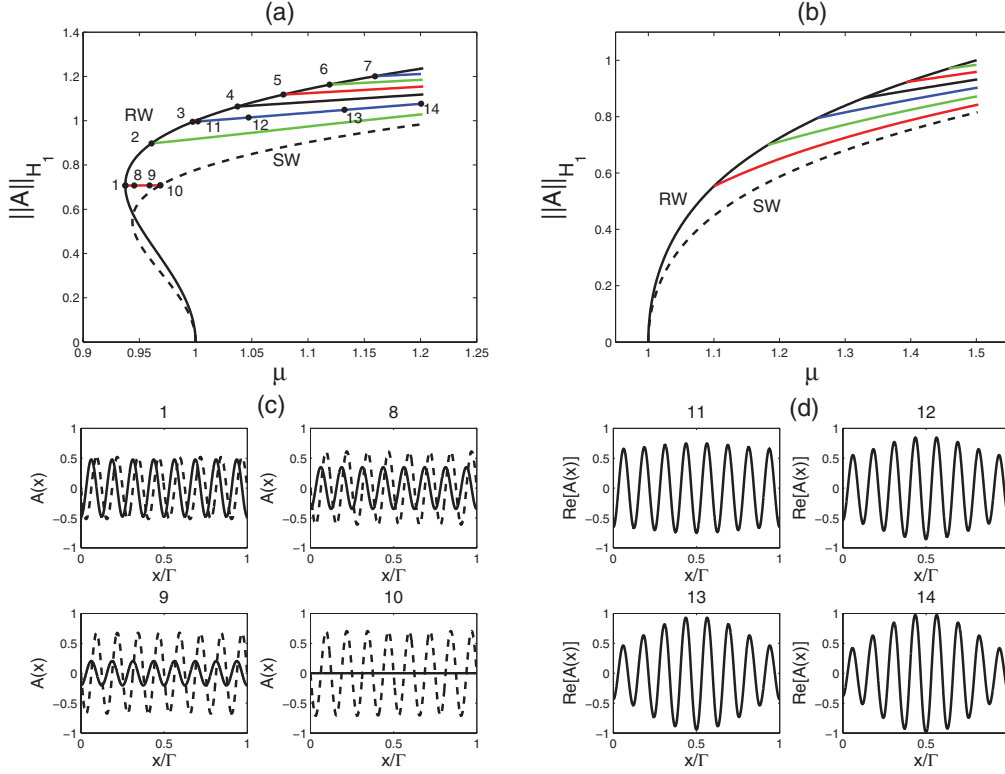


FIG. 16. (Color online) Bifurcation diagrams for (a) subcritical and (b) supercritical stationary solutions with $k = 1$ with several secondary branches of nonuniform states satisfying NBC. (c) Sample profiles of $\text{Re}A(x)$ (solid line) and $\text{Im}A(x)$ (dashed line) along the branch extending between points 1 and 10 in panel (a). (d) Sample profiles of $\text{Re}A(x)$ along the secondary branch bifurcating from the RW branch at point 3 in panel (a). The behavior along the branches bifurcating from points 2 and 4–7 is qualitatively similar to (d). Parameters: $a_1 = 0$, $a_2 = 0$, $\Gamma = 16\pi$. (a) $b = 0.5$. (b) $b = -0.5$.

The stability of the periodic solutions is determined by the eigenvalues of the linearized problem. Writing

$$a(x, t) = \beta_1(t)e^{iqx} + \beta_2^*(t)e^{-iqx}, \quad (35)$$

where $q > 0$ is a real wave number, we find that β_1 and β_2 are complex-valued functions of time satisfying

$$\frac{d}{dt} \begin{pmatrix} \beta_1 \\ \beta_2 \end{pmatrix} = \begin{pmatrix} C_1^+ & C_2^+ \\ C_2^- & C_1^- \end{pmatrix} \begin{pmatrix} \beta_1 \\ \beta_2 \end{pmatrix}, \quad (36)$$

where

$$C_1^\pm \equiv -2\mu + 3k^2 - (b' \pm a_1 q)R_0^2 - (k \pm q)^2, \\ C_2^\pm \equiv -2\mu + 2k^2 - (b' \pm a_2 q)R_0^2.$$

Thus, the eigenvalues of the stability matrix are

$$\sigma_\pm = -g - q^2 \pm \sqrt{(g + q^2)^2 - q^2(f + q^2)}, \quad (37)$$

where

$$f(\mu, k) \equiv (2 + a_2^2 - a_1^2) \{ \mu - k^2 + b' R_0^2 \} \\ + 2\mu - 6k^2 - 4ka_1 R_0^2, \\ g(\mu, k) \equiv 2(\mu - k^2) + b' R_0^2.$$

The location of the eigenvalues for different f and g is shown in Fig. 20. It follows that the periodic solution $A = R_0 \exp i(kx + \phi_0)$ is unstable with respect to perturbations with wave number q , provided

(i) $q^2(f + q^2) < 0$: Both eigenvalues are real and there is only one unstable eigenvalue $\sigma_+ > 0$, yielding the unstable solution

$$\tilde{a}_q(x, t) = e^{\sigma_+ t} [C_2^+ \beta e^{iqx} + (\sigma_+ - C_1^+) \beta^* e^{-iqx}],$$

where β is a complex constant.

(ii) $g + q^2 < 0$ and $q^2(f + q^2) > 0$: The eigenvalues can be either real or complex, but *both* are unstable. The former case applies when $g^2 > q^2(f - 2g)$, leading to unstable solutions of the form

$$\tilde{a}_q(x, t) = e^{\sigma_\pm t} [C_2^\pm \beta e^{iqx} + (\sigma_\pm - C_1^\pm) \beta^* e^{-iqx}],$$

where β is again a complex constant. In contrast, when $g^2 < q^2(f - 2g)$ the eigenvalues are complex, and the unstable solutions take the form

$$\tilde{a}_q(x, t) = e^{\sigma_r t} \{ C_2^+ \beta_1(t) e^{iqx} \\ + [(\sigma_r - C_1^+) \beta_1^*(t) + \sigma_i \beta_2^*(t)] e^{-iqx} \},$$

where

$$\beta_1(t) = \beta \cos(\sigma_i t) + \gamma \sin(\sigma_i t), \\ \beta_2(t) = -\beta \sin(\sigma_i t) + \gamma \cos(\sigma_i t),$$

with β and γ are complex constants. Here $\sigma_r = -g - q^2$, $\sigma_i = \sqrt{(g + q^2)^2 - q^2(f + q^2)}$.

In the following we refer to the instability triggered by real eigenvalues as the Eckhaus instability, since it is associated

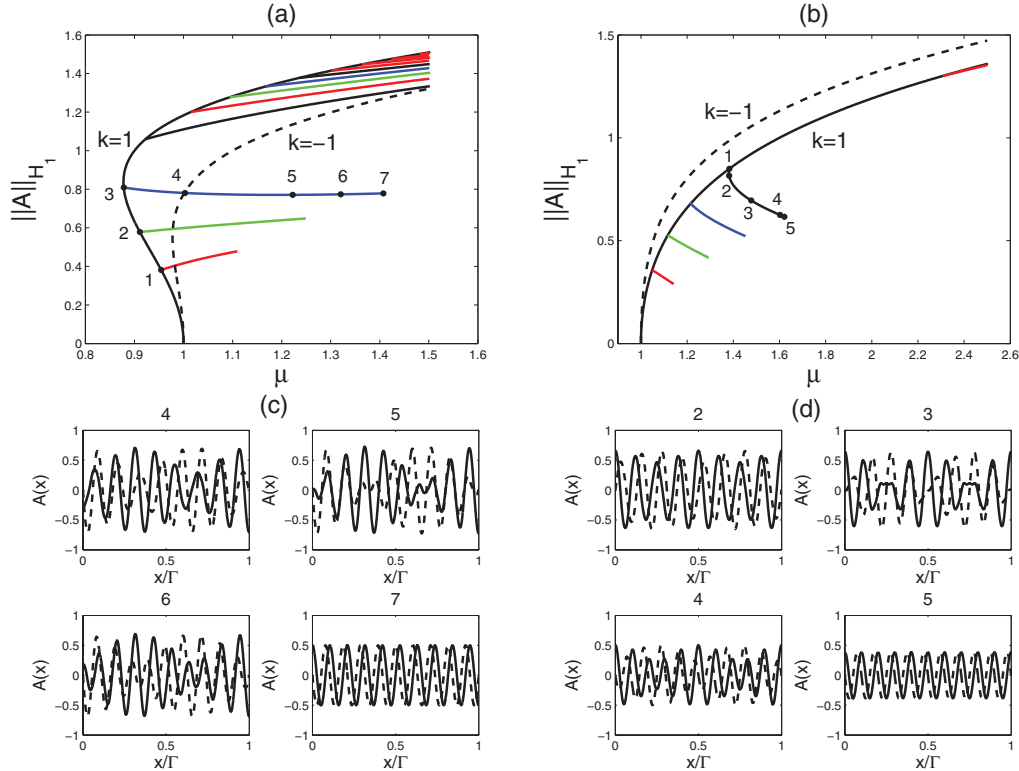


FIG. 17. (Color online) Bifurcation diagrams for (a) subcritical and (b) supercritical stationary solutions with $k = 1$ (RW⁺) and $k = -1$ (RW⁻) together with several secondary branches of nonuniform states satisfying NBC on a domain of length $\Gamma = 16\pi$. Parameters: (a) $b = 0.5$, $a_1 = 0.6$, and $a_2 = 0.8$. (b) $b = -0.5$, $a_1 = 1.4$, and $a_2 = 1.2$. (c) Sample profiles of $\text{Re}A(x)$ (solid line) and $\text{Im}A(x)$ (dashed line) along the branch in (a) bifurcating at point 3 showing a gradual change of wave number between points 3 and 7. $\text{Im}A(x)$ oscillates $\frac{\pi}{2}$ out of phase with $\text{Re}A(x)$. Similar wave-number changes occur along the branches in (a) bifurcating at points 1 and 2. (d) Sample profiles of $\text{Re}A(x)$ (solid line) and $\text{Im}A(x)$ (dashed line) along the branch bifurcating at point 1 in (b) showing a gradual change of wave number between points 1 and 5.

with the appearance of stationary but spatially modulated solutions (cf. Sec. IV). Instability of type (ii) with complex eigenvalues will be called oscillatory modulational instability. To determine the regions in the (k, μ) plane corresponding to stable and unstable solutions on the real line, we determine the conditions under which at least some unstable wave numbers q are present. In this case the conditions (i) and (ii) for instability

can be rewritten as

$$(i) \quad f < 0, \quad (ii) \quad g < \min\{0, f\}. \quad (38)$$

The inequality $g < 0$ can only be satisfied along the R_0^- branch, i.e., (unstable) complex eigenvalues are present only on the R_0^- branch. In contrast, the R_0^+ branch can have only

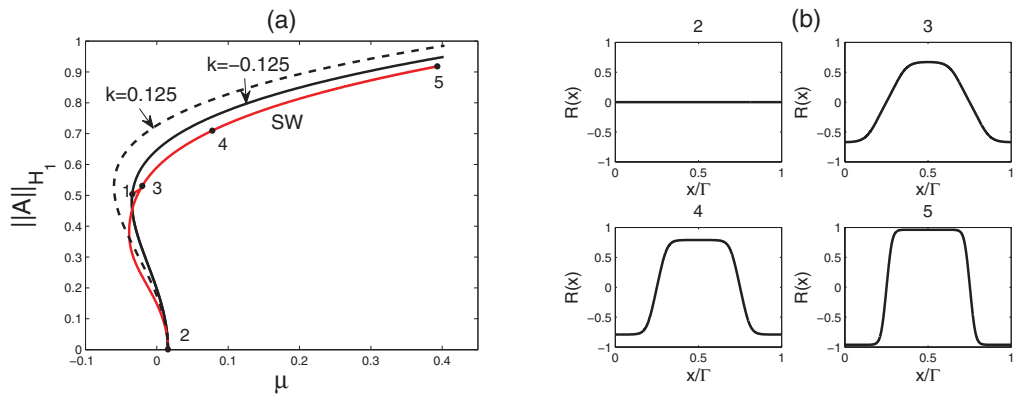


FIG. 18. (Color online) (a) Bifurcation diagram showing the simultaneous bifurcation at $\mu = \frac{1}{64}$ of an SW branch and a pair of RW branches with $k = \pm 0.125$. A secondary branch of spatially modulated states connects the SW and RW⁻ branches between points 1 and 3. (b) Sample profiles of $R(x)$ along the SW branch. Parameters: $b = 0.5$, $a_1 = -0.2$, $a_2 = 0.2$, $\Gamma = 16\pi$.

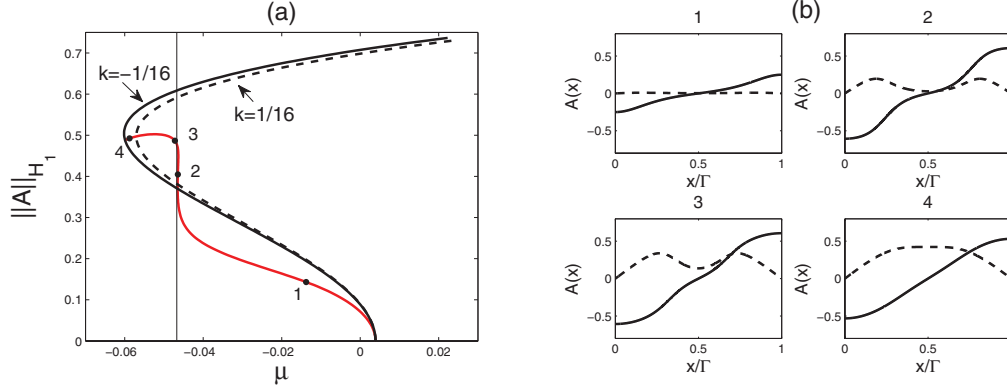


FIG. 19. (Color online) (a) Bifurcation diagram showing the simultaneous bifurcation at $\mu = \frac{1}{256}$ of a branch of two-frequency states [MW: red (gray) curve] undergoing protosnaking and a pair of branches of periodic states RW^\pm with $k = \pm \frac{1}{16}$. The two-frequency states terminate on RW^- . (b) Sample profiles of $\text{Re}A(x)$ (solid line) and $\text{Im}A(x)$ (dashed line) along the MW branch in (a). Parameters: $b = 0.5$, $a_1 = 0.3$, $a_2 = 0.2$, $\Gamma = 16\pi$.

one unstable eigenvalue. We refer to this eigenvalue as the phase eigenvalue.

1. The case $a_1 = a_2 = 0$

In the following we use the notation (1)(i) to refer to case (1) as defined in Sec. V A and condition (i) as defined in Eq. (38), and so on.

We begin with the case $a_1 = a_2 = 0$. In this case, the range of μ within which the periodic wave train is unstable is

(1) (i) and (2) (i):

$$\mu < 2k^2 - \frac{b^2}{8} - \frac{b}{8}\sqrt{b^2 + 16k^2}. \quad (39)$$

Moreover, in order that R_0^+ be present, we also need the conditions $\mu > k^2$ (supercritical case) and $\mu \geq k^2 - b^2/4$ (subcritical case). The resulting instability regions are shown in Figs. 21(a) and 21(c).

(3) (i):

$$k^2 - \frac{b^2}{4} < \mu < k^2. \quad (40)$$

Condition (i) thus holds for all μ along the R_0^- branch [Fig. 21(b)], i.e., R_0^- is unstable.

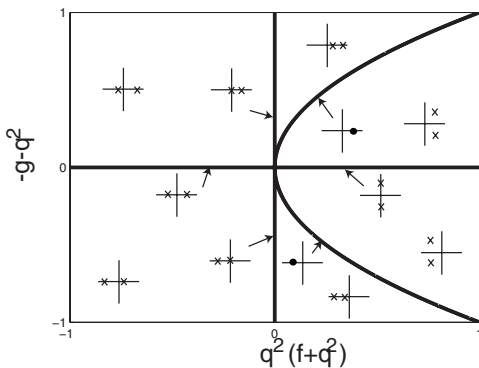
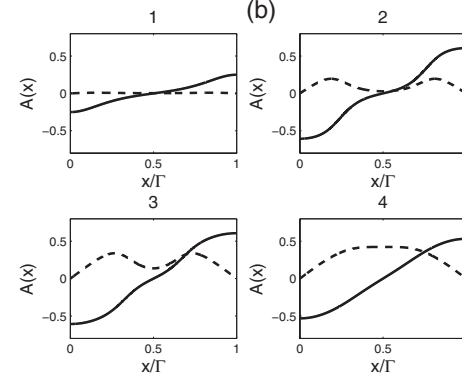


FIG. 20. The position of the eigenvalues σ_\pm in the parameter plane. A Hopf bifurcation takes place along the positive x axis and a saddle-node bifurcation takes place along the y axis.



The resulting bifurcation diagrams resemble those familiar from the supercritical case [13], with amplitude-stable solutions unstable with respect to the Eckhaus instability at small amplitude and stable at large amplitude.

2. The general case

In the general case with at least one of a_1 and a_2 nonzero, we let $\alpha \equiv a_2^2 - a_1^2$ and $s \equiv \sqrt{b^2 + 4(\mu - k^2)}$. To find the range of μ for instability of type (i), we rewrite the condition $f < 0$ as a condition on s . When $\alpha + 4 \neq 0$,

(1) (i) and (2) (i):

$$(4 + \alpha) \left\{ \left[s + \frac{(2 + \alpha)b' - 4ka_1}{4 + \alpha} \right]^2 - \frac{4(b' + 2a_1k)^2 + 16(4 + \alpha)k^2}{(4 + \alpha)^2} \right\} < 0. \quad (41)$$

(3) (i):

$$(4 + \alpha) \left\{ \left[s - \frac{(2 + \alpha)b' - 4ka_1}{4 + \alpha} \right]^2 - \frac{4(b' + 2a_1k)^2 + 16(4 + \alpha)k^2}{(4 + \alpha)^2} \right\} < 0. \quad (42)$$

When $4 + \alpha = 0$, these relations become

(1) (i) and (2) (i):

$$(b' + 2a_1k)(b' + s) + 4k^2 > 0. \quad (43)$$

(3) (i):

$$(b' + 2a_1k)(b' - s) + 4k^2 > 0. \quad (44)$$

We summarize these results in two different types of plots. In the first, we superpose the curves $f = 0$ and $g = f$ on the bifurcation diagram in Fig. 3 showing the amplitude R_0 of a periodic wave train as a function of the wave number k for different values of b and $\mu = 1$ (Fig. 22) and $\mu = -1$ (Fig. 23). Plots of this type determine the range of stable periodic states. We show the same information in the (k, μ) plane in Fig. 24 for $b > 0$ (the subcritical case) and Fig. 25 for $b < 0$ (the supercritical case), in both cases focusing on

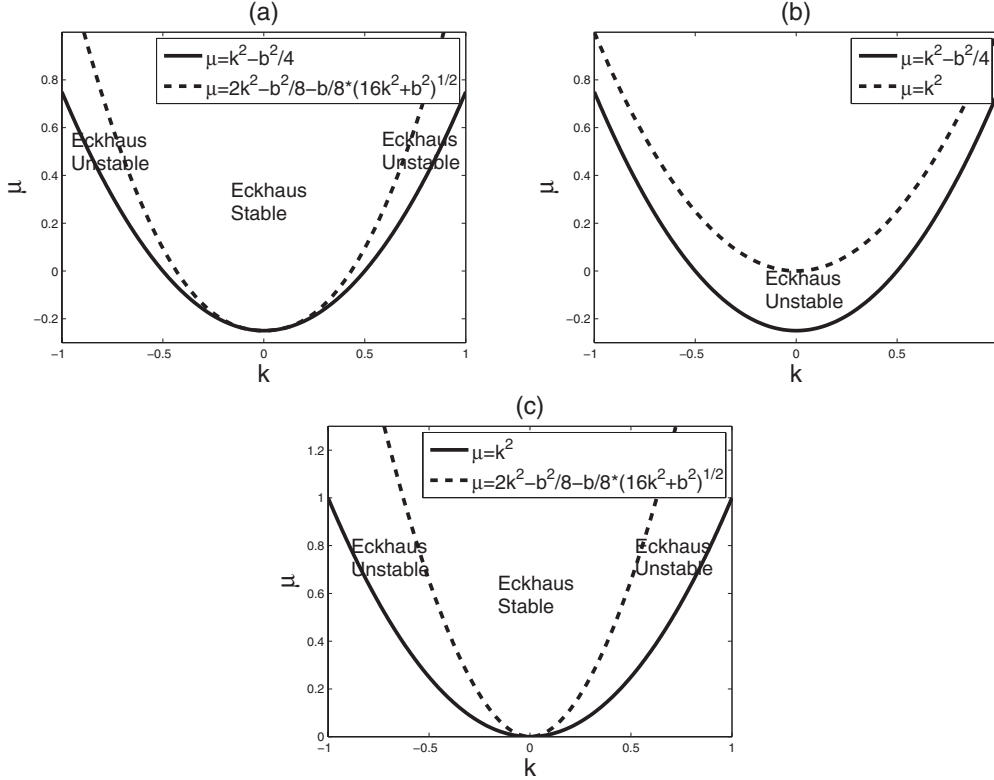


FIG. 21. The (k, μ) plane when $a_1 = a_2 = 0$ and (a) $b = 1$, R_0^+ , (b) $b = 1$, R_0^- , (c) $b = -1$, R_0^+ . When $b \leq 0$ both curves lie in $\mu \geq 0$; when $b > 0$ the curves extend below $\mu = 0$.

the stability properties of the R_0^+ state. In both cases a_2 has been taken to be positive. In each plot we indicate the regions in which a wave train with wave number k is stable with respect to the Eckhaus instability and where it is unstable. These regions are delimited by the union of two curves, the curve $\mu = \mu_{\text{sn}}(k)$ for $|k|$ small (near band center) and the curve $\mu = k^2$ for those wave numbers for which the primary bifurcation is supercritical (larger $|k|$) and by the curve $f = 0$ corresponding to the Eckhaus instability. The resulting plots should be compared with Fig. 21 computed for $a_1 = a_2 = 0$. We see that when $a_1 \neq 0$, $a_2 \neq 0$ the stability region becomes asymmetrical with respect to $k \rightarrow -k$ and may either grow or shrink. Indeed, for some coefficient values the region of stability is suppressed altogether.

The instability regions for the R_0^- branch are more complex since in addition to instability (i), we may also have instability (ii), with either two real positive eigenvalues or a pair of unstable complex eigenvalues. The condition for instability (ii) is

$$\left(1 + \frac{\alpha}{2}\right) s^2 - [(1 + \alpha)b' - 4a_1k]s + \frac{\alpha b'^2 - 8a_1kb' - 16k^2}{2} > 0, \quad (45)$$

subject to the requirement $s < b'$ that defines the existence range for R_0^- . We show the location of complex eigenvalues on the subcritical branch R_0^- for $b > 0$ in Fig. 26 and for $b < 0$ in Fig. 27. Note that complex eigenvalues are only present close to the saddle node where the time scales for the growth of amplitude and phase perturbations become comparable. We also

mention that the quantity $f - 2g = a_2^2 R_0^4 - (a_1 R_0^2 + 2k)^2$ is negative whenever $a_2 = 0$. In this case, the condition for the presence of complex eigenvalues, $g^2 < q^2(f - 2g)$, cannot be satisfied. This is as expected since Eq. (2) is then of gradient type. We leave to future work the possibility that the unstable oscillations present when $a_2 \neq 0$ acquire stability at finite amplitude and the role played by the complex eigenvalues in the stability properties of the various secondary states identified in Sec. IV.

Additional light can be shed on the plots in Figs. 24–27 by examining the special (and simpler) case $k = 0$ (the band center), starting with instability (i). In the supercritical regime the R_0^+ branch is unstable only when $4 + \alpha < 0$, within the range $\mu > -\frac{2(2+\alpha)b^2}{(4+\alpha)^2}$. In the subcritical regime the R_0^+ branch is unstable for all μ when $4 + \alpha \leq 0$. When $-4 < \alpha < 0$ there is a range of instability, $-\frac{b^2}{4} < \mu < -\frac{2(2+\alpha)b^2}{(4+\alpha)^2}$ which shrinks as α increases toward $\alpha = 0$ and vanishes when α reaches zero. The subcritical R_0^- branch is always unstable. The instability (ii) only appears on the R_0^- branch, and then only when $\alpha > 0$ with $-\frac{b^2}{4} < \mu < -\frac{(1+\alpha)b^2}{(2+\alpha)^2}$. These results are reflected in Figs. 24–27.

3. Finite-size effects

In the presence of restrictions on q , e.g., due to a finite domain size, the allowed wave number q limits the range of unstable μ . For example, for periodic boundary conditions with period 2Γ , the wave numbers $k + k_c$ and q must be integer multiples of $\frac{\pi}{\Gamma}$. With $k_c = \frac{\pi}{\Gamma}(N + l)$, where N is a

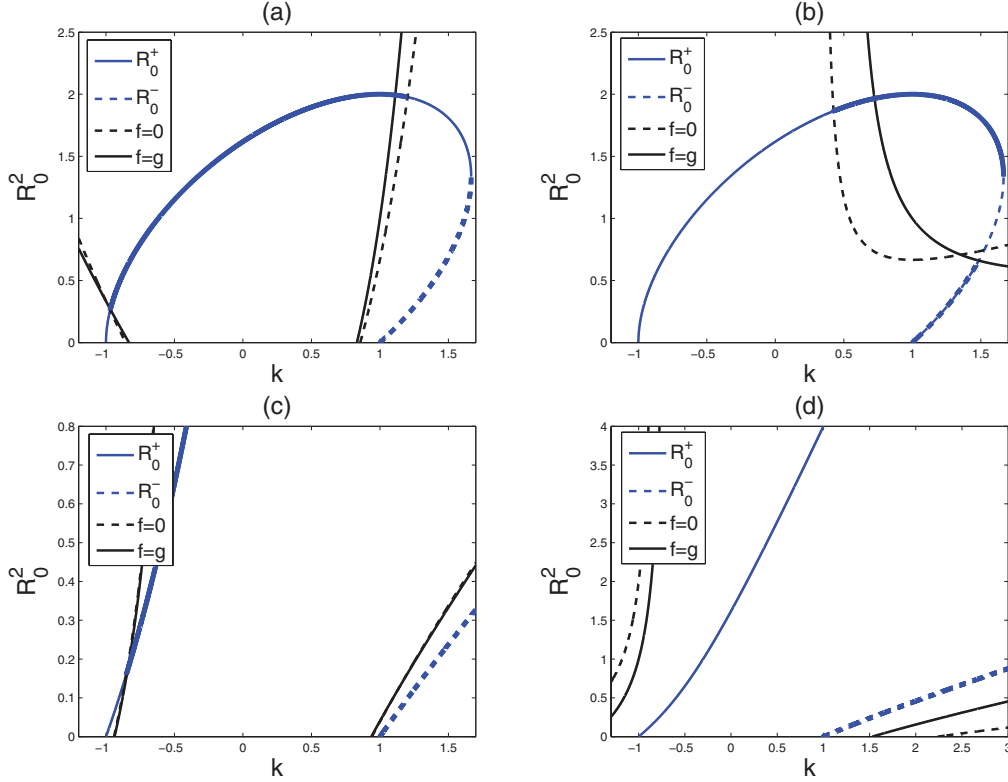


FIG. 22. (Color online) Bifurcation diagrams $R_0^2(k)$ when $\mu = b = 1$ showing the onset of type (i) ($f = 0$, black dashed line) and type (ii) ($g = f$, black line) instabilities. Thick blue (gray) line indicates stable solutions while the thick dashed blue (gray) line indicates the R_0^- solutions unstable with respect to instability (i) only. (a) $a_1 = 3$, $a_2 = 4$. (b) $a_1 = -3$, $a_2 = -2$. (c) $a_1 = 3$, $a_2 = 6$. (d) $a_1 = -3$, $a_2 = 0$.

non-negative integer and $0 \leq l < 1$, the possible values of k and q are $k_n = \frac{\pi}{\Gamma}(n-l)$ and $q_m = \frac{\pi m}{\Gamma}$ with $n \in \mathbb{Z}$ and $m \in \mathbb{N}$, respectively. The smallest unstable wave number q_m is, therefore, finite, cf. Refs. [12,13], resulting in a slight decrease in the range of instability.

B. Stability of secondary branches

We have also examined the stability of the secondary branches by computing numerically the temporal spectrum σ and examining the behavior of the leading eigenvalues along the various branches, focusing primarily on the secondary branches bifurcating from the $k = 0$ branch. Figures 9–15 show that the bifurcation to the first of these is always supercritical when $b > 0$, implying that the first secondary branch has initially a single unstable eigenvalue. When the branch enters the protosnaking region, this eigenvalue becomes very small. If the branch remains monotonic this eigenvalue remains positive but, if the branch undergoes folds, it can become negative, thereby stabilizing the branch. This is so in Figs. 10(b), 12(a), and 14(a). In Fig. 12(a) there are, in fact, four folds on the first secondary branch, the first three of which are not visible on the scale of the figure. In other cases, however, the portion of the branch with positive slope remains unstable. This is the case, for example, in Figs. 13(b) and 13(c).

VI. CONCLUSIONS

In this paper, we have explored in detail the properties of steady solutions of the cubic-quintic Ginzburg-Landau equation [Eq. (2)]. This equation arises in studies of the transition from subcritical to supercritical spatially periodic patterns and is parametrized by the coefficients a_1 , a_2 of cubic derivative terms, in addition to the coefficient b of the cubic term and the wave number of the state or equivalently the domain length Γ . Altogether, we identified *four* critical codimension-one curves in the (a_1, a_2) plane, corresponding to $\beta = 0$ [Eq. (13)], $a_1^2 - a_2^2 = 4$ [Eq. (14)], $(a_2 - a_1)^2 = 4$ [Eq. (17)], and $a_2(a_1 + a_2) = 4$ [Eq. (18)]. Additional codimension-one curves, such as $a_1 + a_2 = 0$ and $a_2 = 0$, can also be significant. Thus, when $a_2 = 0$, the cubic-quintic Ginzburg-Landau equation has gradient structure and, hence, temporal behavior resembling that from the much simpler cubic Ginzburg-Landau equation. This is no longer the case when $a_2 \neq 0$. As a result, temporal oscillations become possible, and nonmonotonic temporal evolution can take place.

We have computed a variety of both primary solution branches corresponding to periodic patterns with either the critical wave number ($k = 0$, band center) or with a shifted wave number ($k \neq 0$, off-center) and determined their stability properties with respect to wavelength changing perturbations of Eckhaus type. We have also computed the different types of secondary branches that result. These correspond, in general, to quasiperiodic states, although on a finite domain both

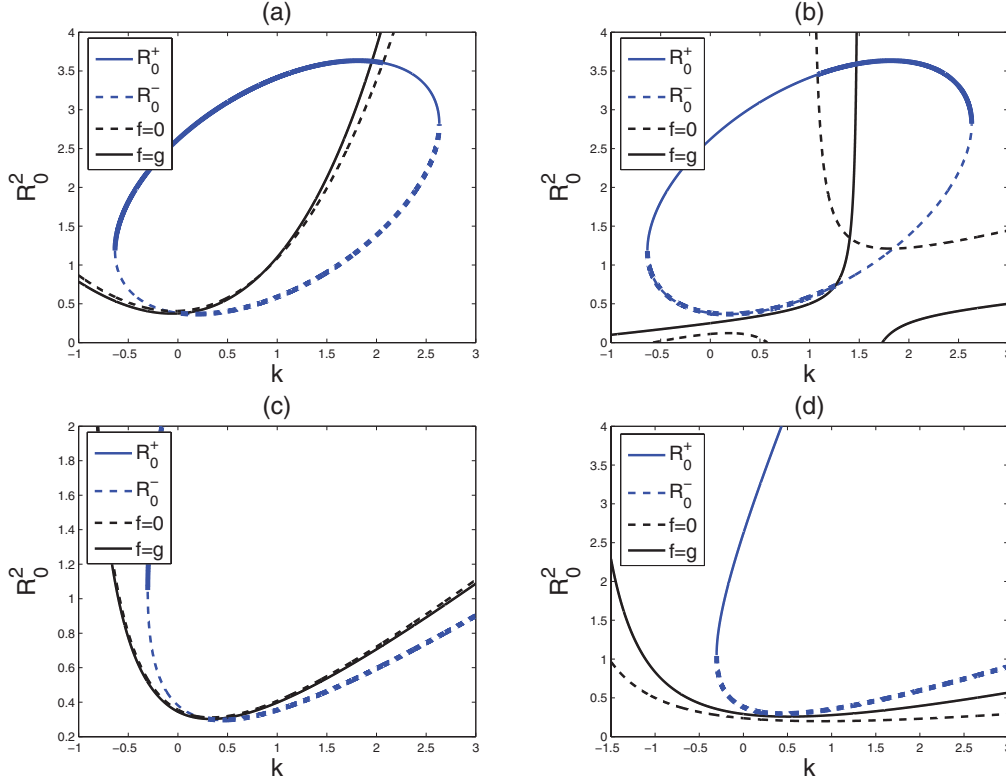


FIG. 23. (Color online) Bifurcation diagrams $R_0^2(k)$ when $\mu = -1$, $b = 3$ showing the onset of type (i) ($f = 0$, black dashed line) and type (ii) ($g = f$, black line) instabilities. Thick blue (gray) line indicates stable solutions while the thick dashed blue (gray) line indicates the R_0^- solutions unstable with respect to instability (i) only. (a) $a_1 = 3$, $a_2 = 4$. (b) $a_1 = -3$, $a_2 = -2$. (c) $a_1 = 3$, $a_2 = 6$. (d) $a_1 = -3$, $a_2 = 0$.

the solution amplitude and phase must, of course, satisfy the boundary conditions. The branches that bifurcate from the primary $k = 0$ branch exhibit protosnaking near a point $\mu = \mu_M$. At this parameter value, one finds a heteroclinic connection between the trivial solution $A = 0$ and a periodic solution $A = R_M \exp ik_M x$ with a well-defined wave number k_M . The presence of these heteroclinic connections, and the associated wave-number selection process, are of particular interest since they play a large role in the interconnections between the $k = 0$ and $k \neq 0$ branches. We have seen, in addition, that the resulting heteroclinic connection may involve either the $R_M^+ \exp ik_M x$ state or the $R_M^- \exp ik_M x$ state, depending on parameters. Since the latter is necessarily amplitude-unstable the resulting front is expected to move to allow the stable state $A = 0$ to invade the domain.

The coefficients a_1 , a_2 that enter the problem near a subcritical bifurcation have a dramatic effect on the shape of the region in the (k, μ) plane containing Eckhaus-stable periodic states. This region, called the Busse balloon in the context of convection, is of great importance in the theory of pattern formation, largely because its existence demonstrates the absence of sharp wave-number selection via any type of instability. In three dimensions, additional instabilities, such as the zigzag, skewed varicose, and oscillatory instabilities, enter the theory and limit the range of stable wave numbers [32], but none leads to sharp wave-number selection in the absence of boundaries, parameter ramps, or fronts. Similar results exist for other spatially periodic patterns, such as hexagons; see,

e.g., Ref. [33]. We have seen that in the present problem the coefficients a_1 , a_2 may render the Eckhaus-stable region highly asymmetrical with respect to $k \rightarrow -k$ and may reduce dramatically its extent, perhaps eliminating it altogether (see, e.g., Fig. 24). This observation is of considerable interest since it describes a mechanism for destabilizing supercritical periodic wave trains at the band center that differs from destabilization caused by coupling to a large-scale mode [34]. We leave to future work the study of this interesting parameter regime.

ACKNOWLEDGMENT

We have benefited from discussions with Y.-P. Ma and L. Tuckerman. This work was supported in part by the National Science Foundation under Grant No. DMS-0908102.

APPENDIX A: HETEROCLINIC AND HOMOCLINIC SOLUTIONS

When $E = L = 0$ and $\mu = \mu_M$, with $b > 0$, $\beta < 0$, the heteroclinic solution connecting the states $A = 0$ and $A = R_M \exp ik_M x$ can be found explicitly:

$$R^2 = -\frac{b}{4\beta} \frac{1}{\exp\left(\mp \frac{bx}{2\sqrt{-\beta}}\right) + 1},$$

$$\phi = \mp \frac{a_1 + a_2}{8\sqrt{-\beta}} \log \left[\frac{1 + \exp\left(\pm \frac{bx}{2\sqrt{-\beta}}\right)}{2} \right]. \quad (\text{A1})$$

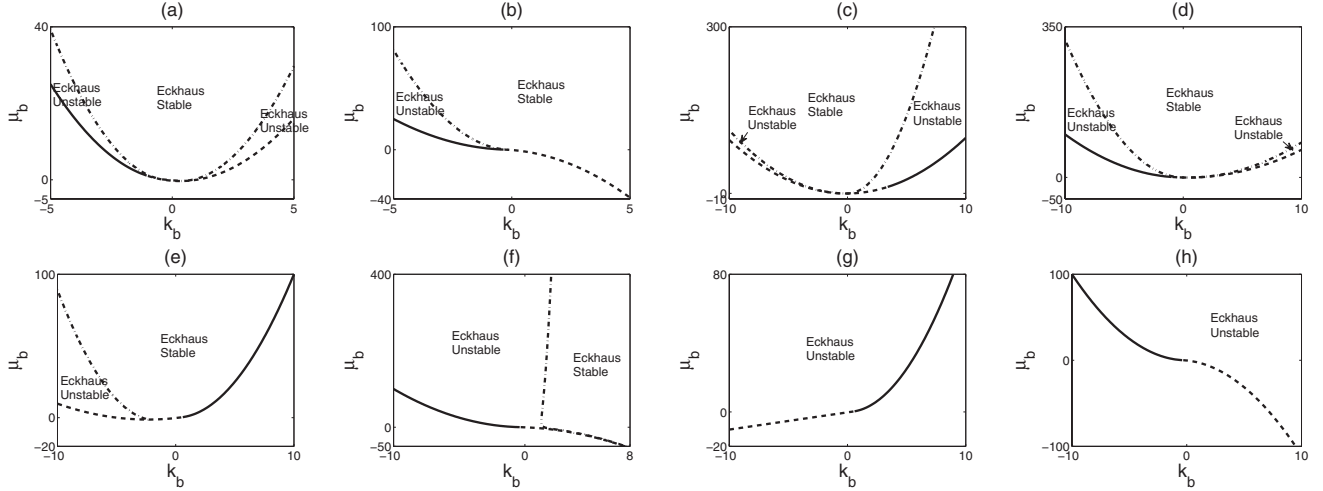


FIG. 24. The parameter range ($k_b \equiv k/|b|, \mu_b \equiv \mu/b^2$) for instability (i) of R_0^+ when $b > 0$ and $a_2 > 0$. Dashed curve: Saddle node. Solid curve: $\mu = k^2$. Dash-dotted curve: Eckhaus boundary. (a) $a_1 = 1, a_2 = 2$ ($\alpha > 0$). (b) $a_1 = -1, a_2 = 2$ ($\alpha > 0$). (c) $a_1 = 1.3, a_2 = 1$ ($-4 < \alpha < 0$). (d) $a_1 = -0.6, a_2 = 0.5$ ($-4 < \alpha < 0$). (e) $a_1 = 2.8, a_2 = 1$ ($\alpha < -4$). (f) $a_1 = -2.1, a_2 = 0.5$ ($\alpha < -4$). (g) $a_1 = 3, a_2 = 1$ ($\alpha < -4$). (h) $a_1 = -2.3, a_2 = 0.5$ ($\alpha < -4$).

Here and hereafter we have omitted arbitrary constants x_0 and ϕ_0 determining the location of the front and its phase at this location. The resulting solution is shown in Fig. 7. This solution remains valid when $\mu_{sn} = \mu_M$, i.e., when the condition (18) holds and the heteroclinic orbit connects the origin to a nonhyperbolic equilibrium (in time).

When $L = 0$ the amplitude R can take on both positive and negative values since the phase ϕ jumps by π each time the amplitude R passes through zero. Thus, homoclinic orbits are present in Figs. 5(a)–5(f), provided the energy E is selected to coincide with the local maximum of the potential $U(R; \mu, L)$. There are three type of homoclinic orbits when $L = 0$:

(1) Homoclinic orbit to the origin: This type of solution occurs when $E = 0$ and $\mu < 0$ and has the form

$$R^2 = \frac{\xi_1 \xi_2}{\xi_1 + (\xi_2 - \xi_1) \cosh^2(\sqrt{-\mu}x)}, \quad (\text{A2})$$

where $\xi_1 = \frac{-b + \sqrt{b^2 - 16\mu\beta}}{4\beta}$ and $\xi_2 = \frac{-b - \sqrt{b^2 - 16\mu\beta}}{4\beta}$. When $\beta < 0$, the coefficient b must satisfy $b > 4\sqrt{\mu\beta}$. The phase varies according to

$$\phi = -\frac{a_1 + a_2}{4\sqrt{\beta}} \tan^{-1} \left(\sqrt{\frac{\xi_1}{-\xi_2}} \tanh \sqrt{-\mu}x \right), \quad \text{if } \beta > 0, \quad (\text{A3})$$

$$\phi = -\frac{a_1 + a_2}{4\sqrt{-\beta}} \tanh^{-1} \left(\sqrt{\frac{\xi_1}{\xi_2}} \tanh \sqrt{-\mu}x \right), \quad \text{if } \beta < 0. \quad (\text{A4})$$

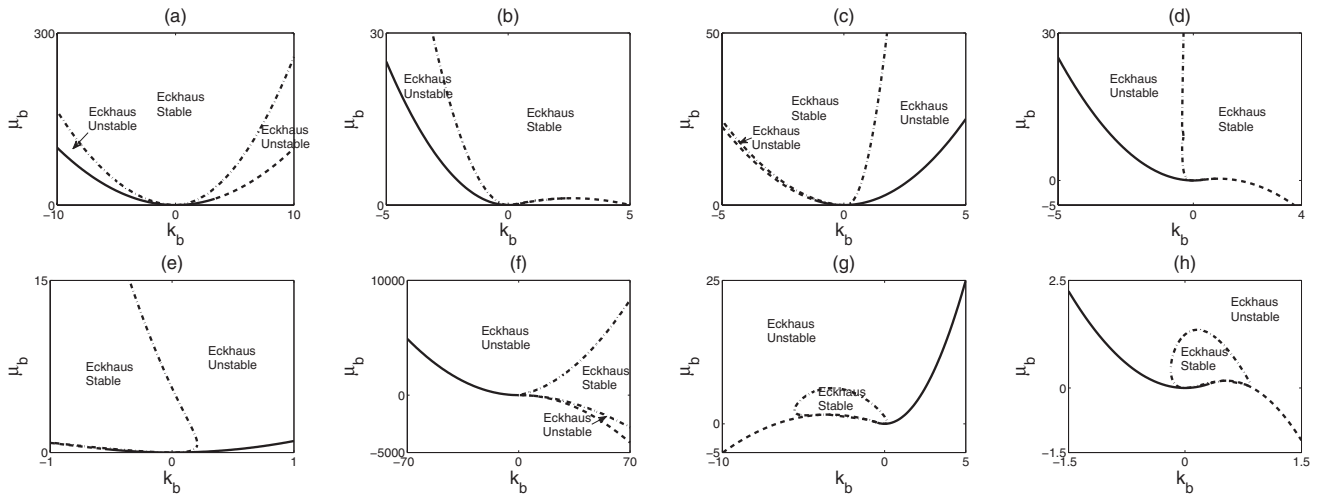


FIG. 25. The parameter range ($k_b \equiv k/|b|, \mu_b \equiv \mu/b^2$) for instability (i) of R_0^+ when $b < 0$ and $a_2 > 0$. Dashed curve: Saddle node. Solid curve: $\mu = k^2$. Dash-dotted curve: Eckhaus boundary. (a) $a_1 = 0.7, a_2 = 1$ ($\alpha > 0$). (b) $a_1 = -0.7, a_2 = 1.5$ ($\alpha > 0$). (c) $a_1 = 1.8, a_2 = 1$ ($-4 < \alpha < 0$). (d) $a_1 = -2.1, a_2 = 0.5$ ($\alpha < -4$). (e) $a_1 = 2.3, a_2 = 0.5$ ($\alpha < -4$). (f) $a_1 = -2.23, a_2 = 0.5$ ($\alpha < -4$). (g) $a_1 = 2.65, a_2 = 0.5$ ($\alpha < -4$). (h) $a_1 = -2.65, a_2 = 0.5$ ($\alpha < -4$).

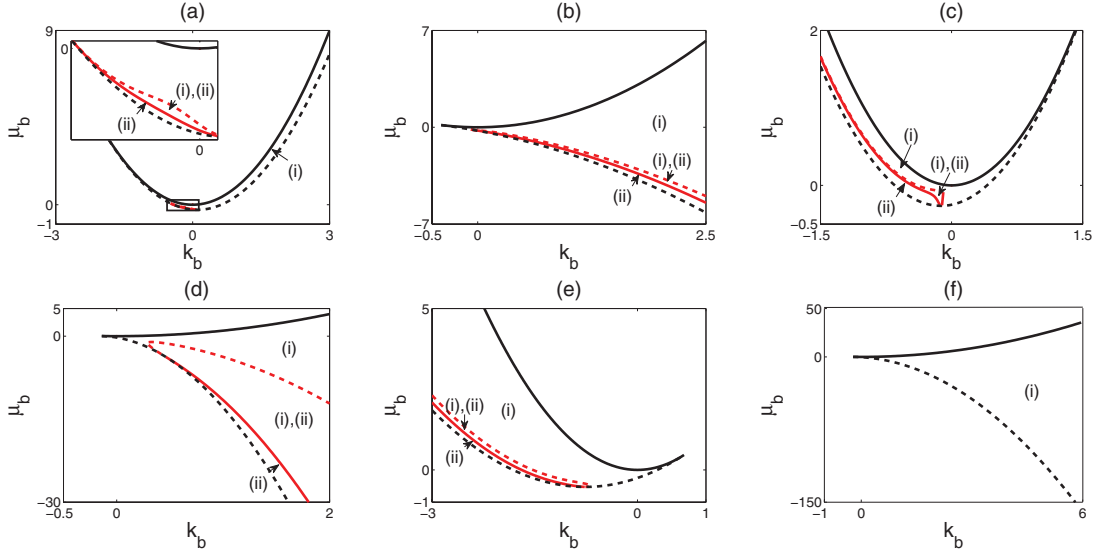


FIG. 26. (Color online) The parameter range ($k_b \equiv k/|b|, \mu_b \equiv \mu/b^2$) for instability (i) and (ii) of R_0^- when $b > 0$ and $a_2 > 0$. Black dashed curve: Saddle node. Black solid curve: $\mu = k^2$. Red (gray) solid curve: boundary of instability (i). Red (gray) dashed curve: boundary of instability (ii). (a) $a_1 = 1, a_2 = 1.4$ ($\alpha > 0$). (b) $a_1 = -1, a_2 = 1.42$ ($\alpha > 0$). (c) $a_1 = 3.46, a_2 = 3$ ($-4 < \alpha < 0$). (d) $a_1 = -3.46, a_2 = 3$ ($-4 < \alpha < 0$). (e) $a_1 = 2.45, a_2 = 1$ ($\alpha < -4$). (f) $a_1 = -3, a_2 = 1.5$ ($\alpha < -4$).

The potential $U(R; \mu, 0)$ for $\beta > 0$ is shown in Fig. 5(a) while that for $\beta < 0$ is shown in Fig. 5(c). In the degenerate case $\mu = 0$, there is a homoclinic orbit that decays algebraically to the origin. This occurs when $E = 0, b < 0$, and $\beta > 0$:

$$R^2 = -\frac{b}{2\beta} \left(1 + \frac{b^2 x^2}{4\beta}\right)^{-1}, \quad \phi = \frac{a_1 + a_2}{4\sqrt{\beta}} \tan^{-1} \left(\frac{bx}{2\sqrt{\beta}}\right). \quad (\text{A5})$$

A typical solution of this form is shown in Fig. 8.

(2) Homoclinic orbit to a nonzero equilibrium crossing $R = 0$:

$$R^2 = \frac{\xi_1 \xi_2 \sinh^2 \left(\sqrt{\mu + \frac{b\xi_1}{2}} x\right)}{\xi_2 \cosh^2 \left(\sqrt{\mu + \frac{b\xi_1}{2}} x\right) - \xi_1}. \quad (\text{A6})$$

Here $\xi_1 = \frac{-b - \sqrt{b^2 - 12\mu\beta}}{6\beta}$, $\xi_2 = \frac{-b + 2\sqrt{b^2 - 12\mu\beta}}{6\beta}$, and $E = U(\sqrt{\xi_1})$ corresponding to the local maximum of U . When $\beta > 0$, μ must be positive with $b < -2\sqrt{3\mu\beta}$. When $\beta < 0$,

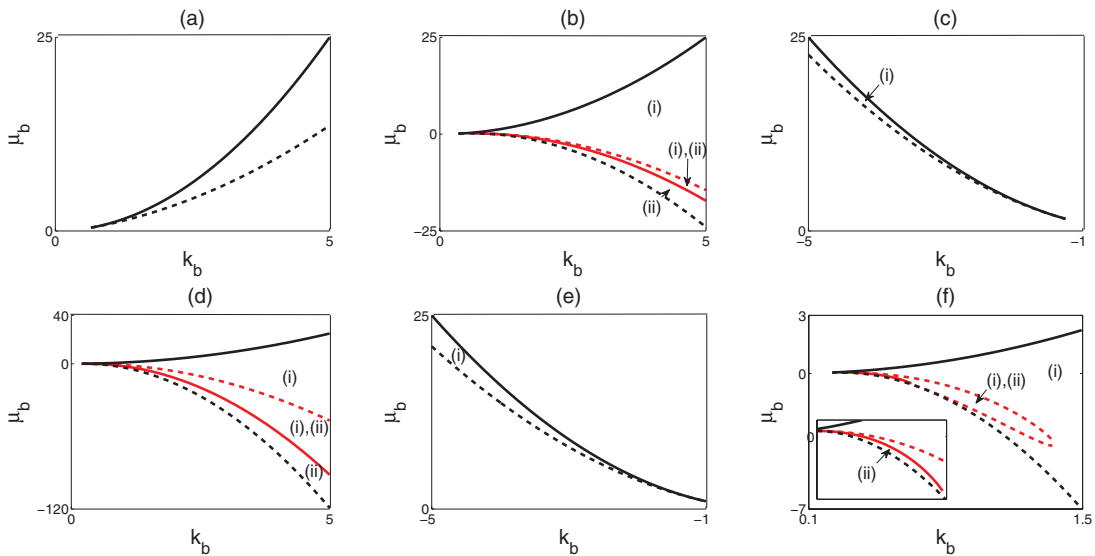


FIG. 27. (Color online) The parameter range ($k_b \equiv k/|b|, \mu_b \equiv \mu/b^2$) for instability (i) and (ii) of R_0^- when $b < 0$ and $a_2 > 0$. Black dashed curve: Saddle node. Black solid curve: $\mu = k^2$. Red (gray) solid curve: boundary of instability (i). Red (gray) dashed curve: boundary of instability (ii). (a) $a_1 = 0.45, a_2 = 2$ ($\alpha > 0$). (b) $a_1 = -1, a_2 = 2$ ($\alpha > 0$). (c) $a_1 = 2.2, a_2 = 1.4$ ($-4 < \alpha < 0$). (d) $a_1 = -2.8, a_2 = 2.2$ ($-4 < \alpha < 0$). (e) $a_1 = 3.2, a_2 = 2.2$ ($\alpha < -4$). (f) $a_1 = -3, a_2 = 1.73$ ($\alpha < -4$).

μ can be either positive or negative. But if μ is negative, b must satisfy $b > 4\sqrt{\mu\beta}$. The phase varies according to

$$\phi = -\frac{(a_1 + a_2)}{4} \left\{ \xi_1 x - \frac{1}{\sqrt{\beta}} \tan^{-1} \left[\frac{\tanh \sqrt{\mu + (b\xi_1)/2x}}{\sqrt{(\xi_2/\xi_1) - 1}} \right] \right\}, \quad \text{if } \beta > 0, \quad (\text{A7})$$

$$\phi = -\frac{(a_1 + a_2)}{4} \left\{ \xi_1 x - \frac{1}{\sqrt{-\beta}} \tanh^{-1} \left[\frac{\tanh \sqrt{\mu + (b\xi_1)/2x}}{\sqrt{1 - (\xi_2/\xi_1)}} \right] \right\}, \quad \text{if } \beta < 0. \quad (\text{A8})$$

The relevant potential $U(R; \mu, 0)$ for $\beta > 0$ is shown in Figs. 5(d) and 5(f) and for $\beta < 0$ in Figs. 5(b) and 5(c).

(3) Homoclinic orbit to a nonzero equilibrium which does not cross $R = 0$:

$$R^2 = \frac{\xi_1 \xi_2 \cosh^2 \left(\sqrt{\mu + \frac{b\xi_1}{2}} x \right)}{\xi_1 + \xi_2 \sinh^2 \left(\sqrt{\mu + \frac{b\xi_1}{2}} x \right)}. \quad (\text{A9})$$

Here ξ_1 and ξ_2 are as in Eq. (A2) above, and $E = U(\sqrt{\xi_1})$ again corresponds to the local maximum of U . When $\beta > 0$, μ must be positive with $b < -2\sqrt{3\mu\beta}$. When $\beta < 0$, μ must be negative with $2\sqrt{3\mu\beta} < b < 4\sqrt{\mu\beta}$. The phase varies according to

$$\phi = -\frac{(a_1 + a_2)}{4} \left[\xi_1 x + \frac{1}{\sqrt{\beta}} \tan^{-1} \left(\sqrt{\frac{\xi_2}{\xi_1} - 1} \tanh \sqrt{\mu + \frac{b\xi_1}{2}} x \right) \right], \quad \text{if } \beta > 0, \quad (\text{A10})$$

$$\phi = -\frac{(a_1 + a_2)}{4} \left[\xi_1 x - \frac{1}{\sqrt{-\beta}} \tanh^{-1} \left(\sqrt{1 - \frac{\xi_2}{\xi_1}} \tanh \sqrt{\mu + \frac{b\xi_1}{2}} x \right) \right], \quad \text{if } \beta < 0. \quad (\text{A11})$$

The relevant potential $U(R; \mu, 0)$ for $\beta > 0$ is shown in Figs. 5(d) and 5(f) and for $\beta < 0$ in Fig. 5(e).

When $L \neq 0$, only homoclinic orbits are present [Figs. 6(a) and 6(c)]. For such an orbit the energy E again coincides with the local maximum of the potential $U(R; \mu, L)$, assumed to be located at $R_1 = \sqrt{\xi_1}$. With ξ_2 and ξ_3 as the other two roots of the polynomial $\xi[E - U(\sqrt{\xi})]$, assumed distinct and different from ξ_1 , a homoclinic orbit with a turning point at $\sqrt{\xi_2}$ has the form:

$$R^2 = \xi_1 + \frac{(\xi_2 - \xi_1)(\xi_3 - \xi_1)}{\xi_2 - \xi_1 + (\xi_3 - \xi_2) \cosh^2 [\sqrt{\beta}(\xi_3 - \xi_1)(\xi_1 - \xi_2)x]} \quad (\text{A12})$$

with the phase

$$\phi = -\frac{(a_1 + a_2)}{4} \left\{ \xi_1 x - \frac{1}{\sqrt{\beta}} \tan^{-1} \left[\left(\frac{\xi_1 - \xi_2}{\xi_3 - \xi_1} \right)^{1/2} \tanh \sqrt{\beta}(\xi_3 - \xi_1)(\xi_1 - \xi_2)x \right] \right\} \quad (\text{A13})$$

$$+ \left(k_\infty + \frac{a_1 + a_2}{4} \xi_1 \right) \left\{ x + \frac{\tan^{-1} \left[\sqrt{\frac{\xi_3(\xi_1 - \xi_2)}{\xi_2(\xi_3 - \xi_1)}} \tanh \sqrt{\beta}(\xi_3 - \xi_1)(\xi_1 - \xi_2)x \right]}{\sqrt{\beta \xi_2 \xi_3}} \right\}, \quad \text{if } \beta > 0,$$

$$\phi = -\frac{(a_1 + a_2)}{4} \left\{ \xi_1 x - \frac{1}{\sqrt{-\beta}} \tanh^{-1} \left[\left(\frac{\xi_1 - \xi_2}{\xi_1 - \xi_3} \right)^{1/2} \tanh \sqrt{\beta}(\xi_3 - \xi_1)(\xi_1 - \xi_2)x \right] \right\}$$

$$+ \left(k_\infty + \frac{a_1 + a_2}{4} \xi_1 \right) \left\{ x + \frac{\tan^{-1} \left[\sqrt{\frac{\xi_3(\xi_1 - \xi_2)}{\xi_2(\xi_3 - \xi_1)}} \tanh \sqrt{\beta}(\xi_3 - \xi_1)(\xi_1 - \xi_2)x \right]}{\sqrt{\beta \xi_2 \xi_3}} \right\}, \quad \text{if } \beta < 0. \quad (\text{A14})$$

Here k_∞ is the wave number at the equilibrium. The relevant potential $U(R; \mu, L)$ for $\beta > 0$ is shown in Fig. 6(c) and for $\beta < 0$ in Fig. 6(a).

APPENDIX B: BIFURCATION ANALYSIS NEAR $\mu = 1$

As already noted, the first primary bifurcation occurs at $\mu = 0$ and generates steady spatially homogeneous states

characterized by wave number $k = 0$. Here we study the second primary instability, characterized by states with wave number $k = \pm 1$.

1. The case $a_1 = a_2 = 0$

When $a_1 = a_2 = 0$, Eq. (2) has the symmetry $O(2) \times O(2)$ with the first $O(2)$ generated by the operations $x \rightarrow x + x_0, A \rightarrow A$ and $x \rightarrow -x, A \rightarrow A$, and the second $O(2)$ generated by the operations $x \rightarrow x, A \rightarrow A \exp i\phi_0$ and $x \rightarrow x, A \rightarrow A^*$. At $\mu = 1$ the trivial state $A = 0$ loses stability at a steady-state bifurcation to modes with wave number $k = \pm 1$. Over \mathbb{C} the multiplicity of the zero eigenvalue is, therefore, 2 while over \mathbb{R} its multiplicity is 4. The bifurcation is thus, properly analyzed as a mode interaction problem and we write

$$A(x, t) = v(t)e^{ix} + w(t)e^{-ix} + \text{h.o.t.} \quad (\text{B1})$$

The symmetries of the problem act on the amplitudes (v, w) as follows:

$$\begin{aligned} x \rightarrow x + x_0 : & \quad (v, w) \rightarrow (ve^{ix_0}, we^{-ix_0}), \\ x \rightarrow -x : & \quad (v, w) \rightarrow (w, v); \end{aligned} \quad (\text{B2})$$

$$\begin{aligned} A \rightarrow e^{i\phi_0} A : & \quad (v, w) \rightarrow (ve^{i\phi_0}, we^{i\phi_0}), \\ A \rightarrow A^* : & \quad (v, w) \rightarrow (\bar{w}, \bar{v}). \end{aligned} \quad (\text{B3})$$

It follows, cf. Ref. [35], that the normal form near $\mu = 1$ is

$$\begin{aligned} \dot{v} &= \lambda v + b_1|v|^2 v + b_2|w|^2 v + \text{h.o.t.}, \\ \dot{w} &= \lambda w + b_2|v|^2 w + b_1|w|^2 w + \text{h.o.t.}, \end{aligned} \quad (\text{B4})$$

where $\lambda = \mu - 1$ and the coefficients $b_1 = b$, $b_2 = 2b$ are real. It follows that near $\mu = 1$ there are two distinct nontrivial solutions corresponding to $(v, w) = (v, 0)$ and $(v, w) = (v, v)$. We refer to these solutions as RW: $A = v \exp ix$ and SW: $A = 2v \cos x$ (see Sec. IV B). The stability of these solutions is determined by the coefficients b_1, b_2 [35].

2. Nonzero a_1 or a_2 (or both)

When a_1 or a_2 is nonzero, Eq. (2) has the smaller symmetry $O(2) \times SO(2)$ generated by the operations $x \rightarrow x + x_0, A \rightarrow A$ and $x \rightarrow x, A \rightarrow A \exp i\phi_0$ and the reflection $x \rightarrow -x, A \rightarrow A^*$. Since the linear problem is unchanged the multiplicity of the zero eigenvalues remains four over \mathbb{R} , but the amplitude equations must now respect the following symmetries:

$$\begin{aligned} x \rightarrow x + x_0 : & \quad (v, w) \rightarrow (ve^{ix_0}, we^{-ix_0}), \\ A \rightarrow e^{i\phi_0} A : & \quad (v, w) \rightarrow (ve^{i\phi_0}, we^{i\phi_0}), \end{aligned} \quad (\text{B5})$$

together with

$$x \rightarrow -x, A \rightarrow A^* : \quad (v, w) \rightarrow (v^*, w^*). \quad (\text{B6})$$

Thus,

$$\begin{aligned} \dot{v} &= \lambda v + b_{11}|v|^2 v + b_{12}|w|^2 v + \text{h.o.t.}, \\ \dot{w} &= \lambda w + b_{21}|v|^2 w + b_{22}|w|^2 w + \text{h.o.t.}, \end{aligned} \quad (\text{B7})$$

where $\lambda = \mu - 1$ and the coefficients $b_{11} = b - a_1 + a_2$, $b_{12} = 2(b - a_2)$, $b_{21} = 2(b + a_2)$, and $b_{22} = b + a_1 - a_2$ are

real. These equations admit a pair of distinct RW solutions $(v, w) = (v, 0)$ and $(v, w) = (0, w)$, hereafter RW⁺: $A = v \exp ix$ and RW⁻: $A = w \exp -ix$, both of which bifurcate from $\mu = 1$. The equations, in addition, admit mixed modes of the form (v, w) , $vw \neq 0$, hereafter MW: $A = v \exp ix + w \exp -ix$, given by

$$|v|^2 = -\lambda(b - a_1 - a_2)/\Delta, \quad |w|^2 = -\lambda(b + a_1 + a_2)/\Delta. \quad (\text{B8})$$

Here $\Delta \equiv 3b^2 + (a_1 - 3a_2)(a_1 + a_2)$ is assumed to be nonzero. These expressions imply that the MW only exist for $|a_1 + a_2| < |b|$, in agreement with the calculation in Appendix C. In particular, when $|a_1 + a_2| = |b|$ the MW degenerate into one or other RW. In contrast, when $a_1 = a_2 = 0$ the RW[±] branches become identical and the MW branch becomes SW, in agreement with the preceding section. In the special case $a_1 = a_2$ the RW[±] branches become identical [cf. Eq. (17)] while in the case $a_1 + a_2 = 0$ the MW become SW with $|v| = |w|$. These results explain the absence of an MW branch in Figs. 17(a) and 17(b) and the presence of an SW branch in Fig. 18. They also explain the presence of an MW branch in Fig. 19, where the MW branch bifurcates simultaneously with the RW[±]. The stability of the above solutions is determined by the coefficients $b_{11}, b_{12}, b_{21}, b_{22}$, although the branches are initially all unstable due to the inherited unstable $k = 0$ eigenvalue.

The above results describe fully the bifurcation behavior near the $k = 1$ primary bifurcation and are readily generalized to $k \neq 0, 1$. Global results based on the particle-in-a-potential formulation are summarized in the corresponding bifurcation diagrams.

APPENDIX C: CALCULATION OF $\frac{dE}{d\mu}$ AND $\frac{dL}{d\mu}$ ON PRIMARY BRANCHES

The direction of branching at the bifurcation point is determined by the sign of the quantity $\frac{dE}{d\mu} - U_{0,L} \frac{dL}{d\mu} - U_{0,\mu}$. This quantity measures the parameter dependence of the energy difference between that of the periodic orbit and the minimum of the potential $U(R; \mu, L)$ and must be of the same sign as $\mu - \mu_0$ for a periodic orbit to be created as μ changes. Here μ_0 is the value of μ at the bifurcation point. Hence, to determine the direction of branching, we need to compute $\frac{dE}{d\mu}$ and $\frac{dL}{d\mu}$. At the bifurcation point, the following conditions hold:

$$U(R_0; \mu_0, L_0) = E_0, \quad U_R(R_0; \mu_0, L_0) = 0, \quad (\text{C1})$$

$$U_{RR}(R_0; \mu_0, L_0) = \frac{2\pi^2 n^2}{\Gamma^2}.$$

The subscript 0 indicates that the quantity is evaluated on the primary branch. If μ is changed by a small amount, $\mu_0 \rightarrow \mu_0 + \delta\mu$, then $E_0 \rightarrow E_0 + \delta E$, $L_0 \rightarrow L_0 + \delta L$, and the position of the local minimum of U will be shifted from R_0 to $R_0 + \delta R_0$. Since $U_R = 0$ along the primary branch, it follows that $\partial_R U(R_0 + \delta R_0; \mu_0 + \delta\mu, L_0 + \delta L) = 0$ and, hence, that

$$\frac{\delta R_0}{\delta\mu} = -U_{RR}^{-1} \left(U_{RL} \frac{\delta L}{\delta\mu} + U_{R\mu} \right). \quad (\text{C2})$$

To calculate the period of amplitude modulation under small perturbation, we need to expand the potential energy locally up to fourth order in $r \equiv R - (R_0 + \delta R_0)$. To simplify expressions, let $U_0 = U(R; \mu_0, L_0)$ with U representing $U(R; \mu_0 + \delta\mu, L_0 + \delta L)$ unless otherwise specified. The potential can be expressed in the form

$$U(R) = U(R_0 + \delta R_0) + \frac{U_{RR}(R_0 + \delta R_0)}{2!} r^2 + \frac{U_{RRR}(R_0 + \delta R_0)}{3!} r^3 + \frac{U_{RRRR}(R_0 + \delta R_0)}{4!} r^4 + O(r^5), \quad (C3)$$

and this expansion employed in the computation of the half period of amplitude modulation: $\int_{R_{\min}}^{R_{\max}} \frac{dR}{\sqrt{E_0 + \delta E - U(R)}}$. To calculate the integral, consider the change of variable

$$\Delta s^2 = U(R) - U(R_0 + \delta R_0), \quad (C4)$$

where $\Delta \equiv E_0 + \delta E - U(R_0 + \delta R_0)$. Then

$$r = \sqrt{\frac{2\Delta}{U_{RR}}} \left[s - \frac{U_{RRR} \Delta^{1/2}}{3\sqrt{2} U_{RR}^{3/2}} s^2 + \frac{(5U_{RRR}^2 - 3U_{RRRR} U_{RR}) \Delta}{36U_{RR}^3} s^3 \right] + O(\Delta^2). \quad (C5)$$

Substituting this expression into the integral yields

$$\sqrt{\frac{U_{RR}}{U_{0,RR}}} - 1 = \frac{5U_{RRR}^2 - 3U_{RRRR} U_{RR}}{24U_{RR}^3} \Delta + O(\Delta^{3/2}), \quad (C6)$$

and, hence,

$$U_{0,RRR} \frac{\delta R_0}{\delta \mu} + U_{0,RRL} \frac{\delta L}{\delta \mu} + U_{0,RR\mu} = \left(\frac{\delta E}{\delta \mu} - U_{0,L} \frac{\delta L}{\delta \mu} - U_{0,\mu} \right) \frac{5U_{0,RRR}^2 - 3U_{0,RRRR} U_{0,RR}}{12U_{0,RR}^2}. \quad (C7)$$

A similar calculation to match the change of phase $\int_{R_{\min}}^{R_{\max}} \frac{kdR}{\sqrt{E-U(R)}}$ yields

$$2 \left(\sqrt{\frac{U_{RR}}{U_{0,RR}}} k_0 - k \right) = \left(\frac{5U_{RRR}^2 - 3U_{RRRR} U_{RR}}{12U_{RR}^3} k_0 - \frac{k_R U_{RRR}}{U_{RR}^2} + \frac{k_{RR}}{U_{RR}} \right) \Delta + O(\Delta^{3/2})$$

and, hence,

$$2 \left(k_R \frac{\delta R_0}{\delta \mu} + \frac{1}{R_0^2} \frac{\delta L}{\delta \mu} \right) = \left(\frac{\delta E}{\delta \mu} - U_{0,L} \frac{\delta L}{\delta \mu} - U_{0,\mu} \right) \left[\frac{U_{0,RRR}}{U_{0,RR}^2} k_R - \frac{k_{RR}}{U_{0,RR}} \right], \quad (C8)$$

where $k \equiv \phi_x$ is a function of R and L . The derivatives in these two relations are all evaluated at the bifurcation point

$\mu = \mu_0$. From the three relations above, we obtain the quantity $\frac{dE}{d\mu} - U_{0,L} \frac{dL}{d\mu} - U_{0,\mu}$ and thereby determine the direction of branching.

The direction of branching of SW can be calculated in the same way. Since the SW are characterized by $L = k = 0$ and are present only as primary bifurcations when $a_1 + a_2 = 0$ (see Sec. IV C), the direction of branching is only determined by $\frac{dE}{d\mu}$, where

$$\frac{dE}{d\mu} = U_{0,\mu} + \frac{12U_{0,RR}^2 (U_{0,RR\mu} - U_{0,RRR} U_{0,RR}^{-1} U_{0,R\mu})}{5U_{0,RRR}^2 - 3U_{0,RRRR} U_{0,RR}} = -\frac{4\mu}{3b}. \quad (C9)$$

Since μ must be positive in order that the bifurcation be from $A = 0$ the direction of branching is determined solely by the sign of b (subcritical if $b > 0$, supercritical if $b < 0$).

The direction of branching of quasiperiodic states that bifurcate from $A = 0$ can also be calculated. These branches appear at $\mu_0 > 0$ when $a_1 + a_2 \neq 0$. The condition $\mu_0 > 0$ implies that $R = 0$ is a local minimum for U when $L = 0$. As L becomes nonzero, U becomes singular at $R = 0$. But since $\mu_0 > 0$, a local minimum of U appears close to $R = 0$. With the change of variable

$$\rho = \frac{R^2}{|L|} - \frac{E}{2\mu'|L|}, \quad (C10)$$

the half period of amplitude modulation and the corresponding phase change can be written as

$$\int_{R_{\min}}^{R_{\max}} \frac{dR}{\sqrt{E-U}} = \frac{1}{2} \int_{\rho_{\min}}^{\rho_{\max}} \frac{d\rho}{\sqrt{\mu'\gamma^2 - 1 - u(\rho; \mu, L, \gamma)}}, \quad (C11)$$

$$\int_{R_{\min}}^{R_{\max}} \frac{kdR}{\sqrt{E-U}} = \frac{1}{2} \int_{\rho_{\min}}^{\rho_{\max}} \frac{\text{sgn}(L)(\rho + \gamma)^{-1} - \frac{a_1 + a_2}{4} |L|(\rho + \gamma)}{\sqrt{\mu'\gamma^2 - 1 - u(\rho; \mu, L, \gamma)}} d\rho, \quad (C12)$$

where $\mu' = \mu + \frac{3a_2 - a_1}{2} L$, $\gamma = \frac{E}{2\mu'|L|}$ and

$$u(\rho; \mu, L, \gamma) = \mu'\rho^2 + \frac{b|L|}{2}(\rho + \gamma)^3 + \beta L^2(\rho + \gamma)^4. \quad (C13)$$

As L tends to 0, these integrals equal to $\frac{\pi}{2\sqrt{\mu_0}}$ and $\frac{\pi}{2}$, respectively, and are independent of γ . To compute the asymptotic behavior of these integrals for small L , we assume that $L = \epsilon \tilde{L}$, $\mu = \mu_0 + \epsilon \tilde{\mu}$ with $\mu_0 = k^2$, and $\gamma = \gamma_0 + \epsilon \tilde{\gamma}$, where $\epsilon \ll 1$. We next define ρ_ϵ by the following relation:

$$\mu'\rho_\epsilon^2 = \mu'\rho^2 + \frac{b|L|}{2}[(\rho + \gamma)^3 - \gamma^3] + \beta L^2[(\rho + \gamma)^4 - \gamma^4],$$

with the property that $\lim_{\epsilon \rightarrow 0} \rho(\epsilon) = \rho$. When ϵ is small,

$$\rho = \rho_\epsilon - \frac{\epsilon b |\tilde{L}|}{4\mu_0} (\rho_\epsilon^2 + 3\rho_\epsilon \gamma + 3\gamma^2) + O(\epsilon^2).$$

Substituting this into the integrals (C11)–(C12), we see that the $O(\epsilon)$ terms give

$$\begin{aligned} 2\tilde{\mu} + (3a_2 - a_1)\tilde{L} + 3\gamma_0 b|\tilde{L}| &= 0, \\ \text{sgn}(L)b + \mu_0\gamma_0(a_1 + a_2) &= 0. \end{aligned} \quad (\text{C14})$$

Since $\gamma_0 > 0$, $\mu_0 > 0$ the sign of L must be the same as $-b(a_1 + a_2)$. As $\epsilon \rightarrow 0$, $\mu_0\gamma_0^2 - 1$ must be positive, implying

that $|b| > \sqrt{\mu_0}|a_1 + a_2|$ in order that a branch of quasiperiodic states exists. Substituting γ into the first relation in Eq. (C14), we obtain a relation between μ and L along the branch, viz.,

$$L = -\frac{2(\mu - \mu_0)}{3a_2 - a_1 - \frac{3b^2}{\mu_0(a_1 + a_2)}} + O(|\mu - \mu_0|^2).$$

This prediction agrees with the result shown in Fig. 19.

-
- [1] E. Knobloch, *Nonlinearity* **21**, T45 (2008).
 [2] H.-G. Purwins, H. U. Bödeker, and Sh. Amiranashvili, *Adv. Phys.* **59**, 485 (2010).
 [3] O. Batiste, E. Knobloch, A. Alonso, and I. Mercader, *J. Fluid Mech.* **560**, 149 (2006).
 [4] T. Ackemann, W. J. Firth, and G.-L. Oppo, *Fundamentals and Applications of Spatial Dissipative Solitons in Photonic Devices*, Advances in Atomic, Molecular, and Optical Physics, Vol. 57, edited by E. Arimondo, P. R. Berman, and C. C. Lin (Academic Press, Burlington, VT, 2009), p. 323.
 [5] A. Yochelis and A. Garfinkel, *Phys. Rev. E* **77**, 035204(R) (2008).
 [6] J. Burke and E. Knobloch, *Chaos* **17**, 037102 (2007).
 [7] A. Bergeon, J. Burke, E. Knobloch and I. Mercader, *Phys. Rev. E* **78**, 046201 (2008).
 [8] J. Burke, A. Yochelis, and E. Knobloch, *SIAM J. Appl. Dyn. Syst.* **7**, 651 (2008).
 [9] S. J. Chapman and G. Kozyreff, *Physica D* **238**, 319 (2009).
 [10] Y. Pomeau, *Physica D* **23**, 3 (1986).
 [11] R. Hoyle, *Pattern Formation* (Cambridge University Press, Cambridge, 2006).
 [12] L. Kramer and W. Zimmermann, *Physica D* **16**, 221 (1985).
 [13] L. S. Tuckerman and D. Barkley, *Physica D* **46**, 57 (1990).
 [14] A. Doelman and W. Eckhaus, *Physica D* **53**, 249 (1991).
 [15] W. Eckhaus and G. Iooss, *Physica D* **39**, 124 (1989).
 [16] J. Burke and E. Knobloch, *Phys. Rev. E* **73**, 056211 (2006).
 [17] M. C. Cross, P. G. Daniels, P. C. Hohenberg, and E. D. Siggia, *J. Fluid Mech.* **127**, 155 (1983).
 [18] F. Dias and G. Iooss, *Eur. J. Mech. B/Fluids* **15**, 367 (1996).
 [19] G. Iooss, A. Mielke, and Y. Demay, *Eur. J. Mech. B/Fluids* **8**, 229 (1989).
 [20] O. Laget and F. Dias, *J. Fluid Mech.* **349**, 221 (1997).
 [21] D. Lo Jacono, A. Bergeon and E. Knobloch, *J. Fluid Mech.* **687**, 595 (2011).
 [22] A. Shepeleva, *Nonlinearity* **11**, 409 (1998).
 [23] L. Yu. Glebsky and L. M. Lerman, *Chaos* **5**, 424 (1995).
 [24] G. Iooss, *C. R. Acad. Sci Paris* **324**, 993 (1997).
 [25] L. Gelens and E. Knobloch, *Eur. Phys. J. D* **59**, 23 (2010).
 [26] E. Knobloch and D. Moore, *Eur. J. Mech. B/Fluids* **10**, 37 (1991).
 [27] J. Duan, P. Holmes, and E. S. Titi, *Nonlinearity* **5**, 1303 (1992).
 [28] E. J. Doedel, A. R. Champneys, T. Fairgrieve, Y. Kuznetsov, B. Oldeman, R. Paffenroth, B. Sandstede, X. Wang, and C. Zhang, *AUTO-07p: Continuation and Bifurcation Software for Ordinary Differential Equations*, available for download from [<http://indy.cs.concordia.ca/auto/>] (2007).
 [29] H. R. Brand and R. J. Deissler, *Phys. Rev. A* **45**, 3732 (1992).
 [30] J. H. P. Dawes, *SIAM J. Appl. Dyn. Syst.* **8**, 909 (2009).
 [31] J. D. Crawford and E. Knobloch, *Nonlinearity* **1**, 617 (1988).
 [32] E. Bodenschatz, W. Pesch and G. Ahlers, *Annu. Rev. Fluid Mech.* **32**, 709 (2000).
 [33] S. Madruga and H. Riecke, *Phys. Rev. E* **75**, 026210 (2007).
 [34] P. C. Matthews and S. M. Cox, *Nonlinearity* **13**, 1293 (2000).
 [35] E. Knobloch, *Phys. Rev. A* **34**, 1538 (1986).